ACS OMEGA

http://pubs.acs.org/journal/acsodf

Article

Improved Catalytic Performances of the NaOH-Treated ZSM-22 Zeolite in the 1-Butene Skeletal Isomerization Reaction: Effect of External Acid Sites

Guoliang Wu, Yunfeng Hu,* Qiang Bao, Jian Zhang, and Junping Ge

Cite This: *ACS Omega* 2023, 8, 14349−14364

Read Online

ACCESS | Metrics & More | Article Recommendations | Supporting Information

ABSTRACT: In this paper, a series of alkaline-treated ZSM-22 zeolite samples were prepared by treating the parent ZSM-22 zeolite using NaOH aqueous solution with different concentrations. By investigating the effects of alkaline treatment on the parent ZSM-22 zeolite, we discovered that the alkaline treatment contributed to the reduction of Brønsted acid sites due to the coverage of extra-framework Al on its external surface. In addition, it was found that the alkaline-treated samples were favorable to the improvement of the isobutene yield and selectivity, while these features appeared to be low for the subsequent acid-washed counterparts in the skeletal isomerization reaction of 1-butene. These results indicate that the catalytic performance of ZSM-22 zeolite is related to reduced amounts of Brønsted acid sites in it. To further reveal the reasons for the promoted catalytic performances of the alkaline-treated ZSM-22 series zeolites, we studied the properties of coke deposited on the two series of samples using Raman spectroscopy and thermogravimetric analysis and mass spectrometry (TG/MS-TPO). It was shown that the carbon deposited on the alkaline-treated series samples was mainly distributed at the outer surface, while the coke was distributed to a relatively lesser extent at the exterior surface for the acid-washed series samples. Moreover, by partially passivating outer acid sites of the parent zeolite, the selected alkaline-treated zeolite, and acid-washed zeolite, their isobutene selectivities were all improved with the decrease in outer acid sites. These phenomena confirmed that the improved catalytic performances of the alkaline-treated samples are related to their decreased external Brønsted acid site density, which further demonstrated that the high isobutene yield and selectivity in the skeletal isomerization reaction of 1-butene is realized via the monomolecular reaction pathway of 1-butene.

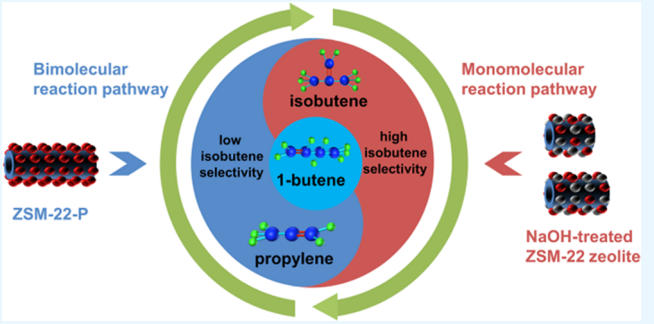

1. INTRODUCTION

Isobutene is an important organic chemical raw material mainly used for the production of methyl *tert*-butyl ether (MTBE), butyl rubber (IIR),[1] poly-isobutene (PIB),[2] *tert*-butyl alcohol,[3] methyl methacrylate (MMA),[4] and so on. Up to now, extensive research has been carried out on the production technology of isobutene using the isomerization method. The major techniques include the addition of isomerization components into the cracking catalyst to improve the isobutene yield in pyrolysis gas,[5] the dehydroisomerization of *n*-butane,[6] and the skeletal isomerization of 1-butene.[7] Although the isobutene yield can be greatly improved in the first process, this technology is highly dependent on the processing conditions and overall layout of the refinery plants, and so its practical application is limited. The direct formation process of isobutene from *n*-butane involves two reactions: the dehydrogenation of *n*-butane and the skeletal isomerization to butene. Dehydroisomerization has to be performed at high temperatures because of its endothermicity,[8] but high temperature is prone to cause side reactions leading to deactivation,[9] and so it is difficult to achieve this process economically. Thus, the skeletal isomerization reaction of 1-butene became the most promising method for increasing the production of isobutene.

So far, many types of catalysts have been studied for the skeletal isomerization of 1-butene. Houžvička et al.[10] and Gao and Moffat[11] prepared catalysts possessing isomerization activities by loading phosphoric acid and 12-tungstophosphoric acid onto silica, respectively. In addition, halogen-modified alumina catalysts can also induce the skeletal isomerization reaction of 1-butene.[12,13] Also, materials with ordered mesoporous pore structures such as MCM-41 and KIT-1 have been investigated.[14] However, as for the catalysts mentioned above, either their selectivities are not high or their stabilities are poor. Compared with most amorphous and

Received: August 25, 2022
Accepted: April 3, 2023
Published: April 11, 2023

mesoporous catalysts, zeolite can trigger the skeletal isomerization reaction of 1-butene to isobutene at a lower reaction temperature.[15] Moreover, zeolite catalysts are also believed to be capable of adjusting the target product selectivity by tuning their pore sizes.[16] It has been found that zeolite catalysts with 10-ring pore structures are especially suitable for the skeletal isomerization of 1-butene because they could facilitate the diffusion of isobutene and inhibit the formation of dimers.[17] For example, FER,[18,19] MFI,[20] MTT,[21] AEL,[22] and TON[23] types of topologies with 10-ring channels have been reported for the skeletal isomerization reaction of 1-butene. Among them, FER zeolite is the most widely used in the reaction of 1-butene into isobutene.[24−26] However, FER zeolite is confronted with the problem of a low isobutene selectivity in the initial reaction stage.[19,27] The advantage of the ZSM-22 zeolite with a TON-type topology is that it exhibits high isobutene selectivity in a short time under appropriate reaction conditions.[28] However, it is noteworthy that the high isobutene selectivity of the ZSM-22 zeolite can be achieved only when operating at harsh conditions, *e.g.*, reactant diluted with an inert gas, high space velocity,[29,30] and high reaction temperature.[31] Therefore, when ZSM-22 zeolite is applied to the skeletal isomerization reaction of 1-butene in industrial manufacturing, if satisfies the requirement of high isobutene selectivity, but entails an increase in separation cost, reaction energy consumption, and bed pressure drop. Therefore, it is necessary to improve the isobutene selectivity of ZSM-22 zeolite in the skeletal isomerization reaction of 1-butene under relatively mild conditions.

Up to now, methods for improving the isobutene selectivity of ZSM-22 zeolite have been reported in numerous studies. Asensi et al.[32] found that the isobutene selectivity of ZSM-22 zeolite depended on its Brønsted acid strength. Byggningsbacka et al.[29] prepared Fe-ZSM-22 zeolite with weaker acid strength by isomorphous substitution, and the results showed that Fe-ZSM-22 zeolite exhibited higher isobutene selectivity. In addition, phosphorus and boron can also poison the strong acid sites of ZSM-22 zeolite by the impregnation method, and boron modification only poisoned the strong acid sites, which avoided the occurrence of side reactions and then improved isobutene selectivity.[31] Moreover, the acid contents of ZSM-22 zeolite also affect the selectivity of isobutene. The isobutene selectivity of Mg-ZSM-22 zeolite was improved by reducing the acid contents using steam treatment or nitric acid treatment.[33] The isobutene selectivity can also be improved by partially passivating the external acid sites of ZSM-22 zeolite.[34] Noteworthily, although the above-mentioned modification methods can improve the isobutene selectivity to a certain extent, remarkable isobutene selectivity was either achieved under more demanding conditions or accompanied by the loss of isobutene yield. To overcome these drawbacks, we tried to improve the isobutene selectivity of ZSM-22 zeolite under mild reaction conditions and without the reduction of isobutene yield and then explore the reason for improving isobutene selectivity.

In this paper, we adopted the method of alkaline treatment to reduce the external Brønsted acid site density of ZSM-22 zeolite, and also, the reason for this decrease in alkaline-treated ZSM-22 zeolite was revealed. It was found that the alkaline-treated ZSM-22 zeolite can effectively improve the yield and selectivity of isobutene. Finally, the effect of external acid sites of the ZSM-22 zeolite on its catalytic performance was discovered by evaluating the catalytic performance of the subsequent acid-washed ZSM-22 series samples, exploring the coke properties of the used samples and partially passivating the outer acid sites of ZSM-22 series samples, respectively.

2. EXPERIMENTAL SECTION

2.1. Parent ZSM-22 Zeolite. The as-synthesized ZSM-22 zeolites preserving the template agent were supplied by Zhuoran Environmental Protection (Dalian) Co., Ltd. They were first calcined in static air at 600 °C for 6 h to remove the template agent. The H-form ZSM-22 zeolite was then produced by two consecutive ion exchanges with 1 mol·L^{-1} NH_4Cl solution at 80 °C for 4 h and calcined again in static air at 600 °C for 6 h. The resulting product was designated as ZSM-22-P.

2.2. NH_4-Form Uncalcined ZSM-22 and H-Form Calcined ZSM-22 Zeolites. In order to obtain NH_4-form uncalcined ZSM-22 zeolites, the as-synthesized ZSM-22 zeolites preserving the template agent were directly treated by two consecutive ion exchanges with NH_4Cl solution. H-form calcined ZSM-22 zeolites were obtained by calcining the NH_4-form uncalcined ZSM-22 zeolites directly. The ion exchange or calcination procedure involved in the preparation process of these two samples was consistent with that described in Section 2.1.

2.3. Post-Treatments. *2.3.1. Alkaline Treatment of the Parent ZSM-22 Zeolite.* The alkaline treatment conditions of the parent ZSM-22 zeolite (ZSM-22-P) are described as follows. First, the template agent was removed by calcination treatment under static air at 600 °C for 6 h. Subsequently, the calcined samples were blended with NaOH aqueous solution (10 mL·g^{-1}, 0.1−1.5 mol·L^{-1}) for 2 h at 80 °C, followed by filtration, washing with deionized water, and drying at 100 °C for 12 h. The obtained solids were converted into the H-form by ion exchanges twice in 1 mol·L^{-1} NH_4Cl solution at 80 °C for 4 h, followed by calcination in static air for 6 h at 600 °C. The resulting product was denoted as ZSM-22-*x*, where *x* represents the concentration of NaOH aqueous solution.

2.3.2. Sequential Acid Washing of Alkaline-Treated ZSM-22 Series Zeolites. Each NaOH-treated sample was subjected to acid washing in 0.1 mol·L^{-1} HCl aqueous solution at 60 °C for 2 h, with 10 g·L^{-1}. The resulting product was washed with distilled water until neutral pH and dried at 100 °C for 12 h. The samples subjected to the acid-washing treatment were denoted with the suffix H. As an example of the sample notation, the NaOH-treated samples treated with acid washing were denoted as ZSM-22-*x*-H. All of the acid-washed samples were converted to the protonic form, as described in Section 2.1.

2.3.3. Partial Passivation of the Outer Acid Sites of ZSM-22 Series Zeolites. The partial passivation of the outer acid sites of ZSM-22 series zeolites was carried out by the chemical liquid deposition (CLD) method adapted from the literature.[35] First, 1.5 g of H-form ZSM-22 zeolite (or NH_4-form uncalcined ZSM-22 zeolite) was mixed with 250 mL of cyclohexane at 30 °C for 10 min under stirring. Then, 3 mL of tetraethyl orthosilicate (TEOS) was added to the mixture, and the reaction was continued for 1 h under agitation. Subsequently, cyclohexane was removed by evacuation at 70 °C. The resultant powder was dried at 100 °C for 12 h, followed by calcination in air at 550 °C for 3 h. The resulting solid samples were denoted with the prefix M. For example, M−ZSM-22-P implied that the ZSM-22-P sample was subjected to partial passivation of external acid sites.

https://doi.org/10.1021/acsomega.2c05478
ACS Omega 2023, 8, 14349−14364

2.4. Characterization Methods of ZSM-22 Series Zeolites. The crystal structure of ZSM-22 series samples was determined with a TD-3500 X-ray diffractometer operating at 35 mA and 40 kV and using Cu Kα radiation. The relative crystallinities of all ZSM-22 series zeolite samples were obtained by calculating the total intensities of peaks (2θ = 8.14 ± 0.14, 20.34 ± 0.14, 24.24 ± 0.12, and 25.70 ± 0.18°), where ZSM-22-P was used as a reference sample. The Si/Al molar ratios were measured by inductively coupled plasma optical emission spectroscopy (ICP-OES, ICPS-7510). Before ICP-OES measurements, about 20 mg of ZSM-22 series samples was dissolved in HF and then diluted using deionized water to 500 mL. A Zeiss SIGMA field-emission scanning electron microscope (FE-SEM) was used to observe their morphologies. Transmission electron microscopy (TEM) was performed with a Tecnai G2 F30 instrument operated at 200 kV. Their textural properties were obtained from N_2 adsorption−desorption isotherms measured at −196 °C using a 3H-2000PM1 specific surface and pore size analyzer after the test samples were degassed under vacuum at 200 °C for 3 h. The specific surface area was calculated according to the Brunauer−Emmett−Teller (BET) method. The total pore volume was dependent on the adsorbed N_2 volume at a relative pressure of approximately 0.99. The external specific surface area and micropore volume were obtained using the *t*-plot method. The BJH method was used to determine the mesopore size distribution. The acidity properties of H-form ZSM-22 series samples were determined by temperature-programmed desorption of ammonia (NH_3-TPD). Specific experimental details are presented in the literature.[18] To distinguish the type of acid sites, FTIR spectra were recorded at 4 cm^{-1} resolution using a Bruker TENSOR27 in-situ spectrometer. Prior to measurements, the samples were pretreated at 400 °C for 3 h. Then, FTIR spectra in the νOH regions were recorded at 150 °C. Subsequently, pyridine vapor was exposed to wafer at ambient temperature for 10 min and equilibrated for 20 min; next, it was outgassed at 150 °C for 30 min to remove excess pyridine molecules. Then, the pyridine-adsorbed infrared spectra (Py-IR) were recorded at 150 °C. FTIR spectroscopy experiments of the adsorbed collidine (2,4,6-trimethylpyridine) were performed on a Thermo fisher Nicolet iS50 spectrometer. The test conditions were the same as those for Py-IR, except that the pretreatment temperature was 350 °C. X-ray photoelectron spectroscopy (XPS) measurements were performed with a Thermo Scientific K-Alpha photoelectron spectrometer with Al Kα irradiation (1486.6 eV). The C 1s peak at a binding energy at 284.8 eV was used to calibrate the binding energy scale. All of the obtained XPS spectra were split using XPS PEAK software, and deconvolution was realized by Gaussian−Lorentzian band shapes. The Raman spectra were obtained on a LabRAM HR Evolution Raman spectrometer using an excitation source of 532 nm. Thermogravimetric analysis (TGA) was performed on a PerkinElmer TGA4000 instrument with a heating rate of 20 °C·min^{-1} under air or helium flow rate of 20 mL·min^{-1}. The products released by coke or the template were detected by a combination of thermogravimetric analysis and mass spectrometry (TG/MS-TPO).

2.5. Catalytic Performance Evaluation of ZSM-22 Series Zeolites. Evaluations of all of the tested ZSM-22 series zeolite catalysts were performed using 1-butene (99.99% purity) as the reactant at atmospheric pressure, 400 °C, and 14 h^{-1}. Typically, 0.5 g of zeolite catalyst (40−60 mesh) was loaded between layers of 40−60 mesh quartz sand in a 1 cm i.d. × 40 cm stainless steel reactor tube. Then, the zeolite catalyst was routinely activated under flowing N_2 (40 mL·min^{-1}) at 400 °C for 0.5 h. Then, a pure 1-butene stream was fed into the reactor containing the zeolite catalyst at the same temperature. After passing through the gas−liquid separator, the gaseous products were analyzed in a GC-8A gas chromatograph (20% sebacic dinitrile/APW (80−100 mesh) packed column, 9 m × 3 mm, FID detector). Considering that the double-bond shift and cis−trans isomerization of *n*-butenes achieve equilibrium before the skeletal isomerization,[36] and isobutene could also be produced by *cis*-2-butene,[37] all linear butenes were regarded as reactants. Thus, the 1-butene conversion was calculated from the consumed *n*-butenes and the selectivity to isobutene from the mass of produced isobutene divided by the mass of consumed *n*-butenes.

3. RESULTS AND DISCUSSION

3.1. Effects of NaOH Treatment. *3.1.1. Structure, Composition, and Morphology.* X-ray diffraction (XRD) patterns of the parent ZSM-22 zeolite (ZSM-22-P) and NaOH-treated series zeolite samples (ZSM-22-*x*) are shown in Figure 1. All of the tested samples have a typical TON

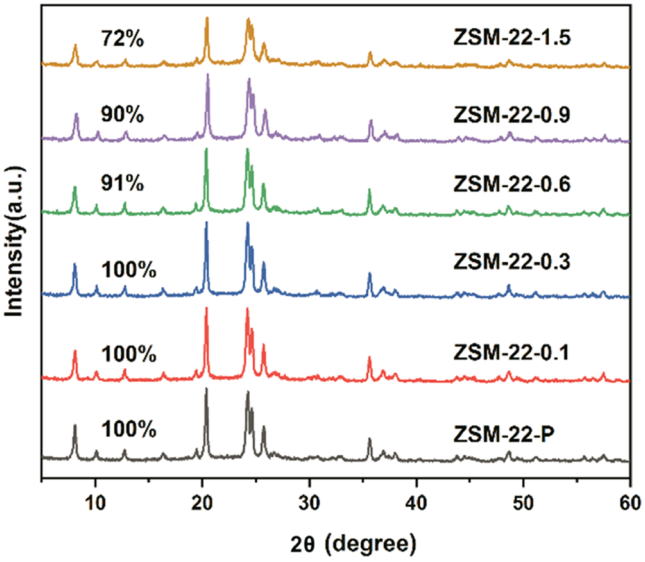

Figure 1. XRD patterns of ZSM-22-P and ZSM-22-*x* series samples.

topological structure.[38,39] Clearly, the samples treated with a low-concentration NaOH aqueous solution preserved good TON-type topologies, but severe treatment resulted in their lower crystallinities. In order to further study the effect of alkaline treatment on the ZSM-22-P sample, the morphologies of ZSM-22-P and ZSM-22-*x* series samples were characterized by SEM. As shown in Figure 2, the morphologies of all samples comprised agglomerates of individual rod-shaped crystals. However, it should be noted that with the increase of alkaline aqueous concentration, the agglomerated crystals of ZSM-22-P sample began to dissolve, especially for ZSM-22-0.9 and ZSM-22-1.5 samples. In the TEM images shown in Figure 3, the presence of intracrystalline mesopores (average size: 6.7 nm) was clearly observed for ZSM-22-0.9 and ZSM-22-1.5 samples with respect to the ZSM-22-P sample, and the crystal edges of ZSM-22-0.9 and ZSM-22-1.5 samples became rougher. These phenomena indicate that the desilication of the ZSM-22-P

https://doi.org/10.1021/acsomega.2c05478
ACS Omega 2023, 8, 14349−14364

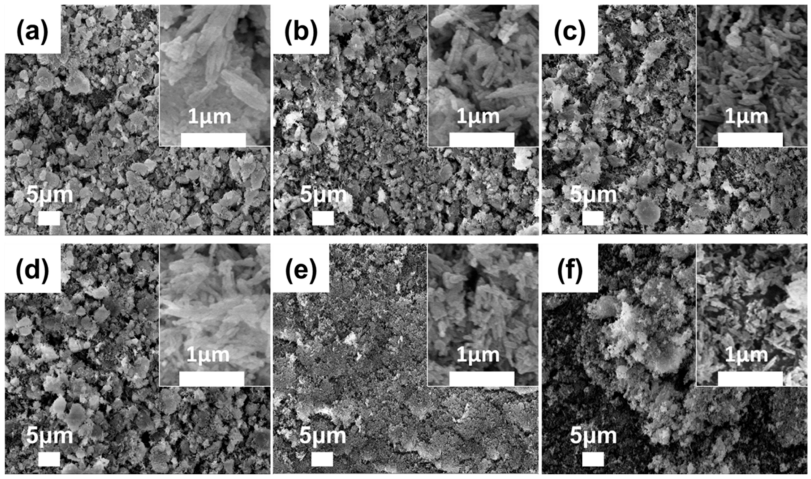

Figure 2. SEM images of ZSM-22-P and ZSM-22-*x* series samples: (a) ZSM-22-P, (b) ZSM-22-0.1, (c) ZSM-22-0.3, (d) ZSM-22-0.6, (e) ZSM-22-0.9, and (f) ZSM-22-1.5.

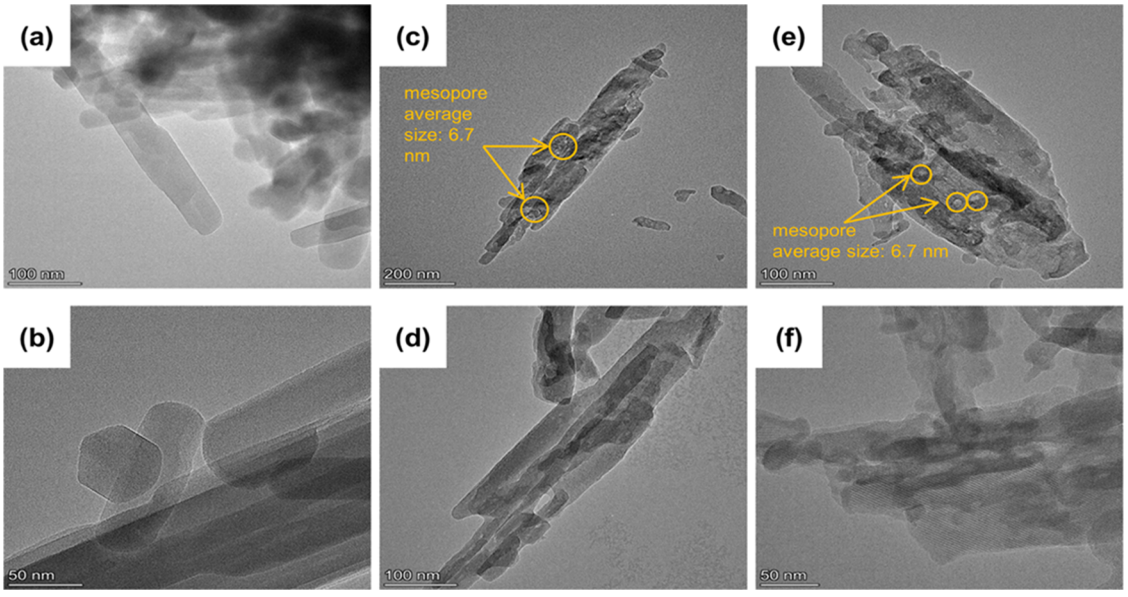

Figure 3. TEM images of ZSM-22-P and ZSM-22-*x* series samples. (a, b) ZSM-22-P, (c, d) ZSM-22-0.9, and (e, f) ZSM-22-1.5.

Table 1. Composition and Textural Properties of ZSM-22-P and ZSM-22-*x* Series Samples

sample	Si/Al[a]	S_{BET} ($m^2 \cdot g^{-1}$)[b]	S_{exter} ($m^2 \cdot g^{-1}$)[c]	V_{micro} ($mL \cdot g^{-1}$)[c]	V_{total} ($mL \cdot g^{-1}$)[d]	V_{meso} ($mL \cdot g^{-1}$)[e]
ZSM-22-P	53	140	31	0.06	0.23	0.17
ZSM-22-0.1	63	85	39	0.03	0.20	0.17
ZSM-22-0.3	56	84	46	0.02	0.21	0.19
ZSM-22-0.6	57	145	46	0.05	0.26	0.21
ZSM-22-0.9	44	108	52	0.03	0.25	0.22
ZSM-22-1.5	25	140	79	0.03	0.34	0.31

[a]Silicon-to-aluminum (Si/Al) molar ratios were measured by ICP-OES. [b]Determined by BET equation. [c]Determined by the *t*-plot method applied in the thickness range of 0.43−0.64 nm. [d]Calculated from the N_2 volume adsorbed at $P/P_0 = 0.99$. [e]Determined by subtracting the microporous volume from the total pore volume.

sample was caused by alkaline treatment. The decreased Si/Al ratios of ZSM-22-0.9 and ZSM-22-1.5 samples shown in Table 1 also confirm this conclusion. However, the Si/Al ratios were almost unchanged for the alkaline-treated samples modified by NaOH aqueous solution with low concentration, and so further investigation is needed.

The nitrogen adsorption and desorption isotherms of ZSM-22-P and ZSM-22-*x* series samples are shown in Figure 4a. The uptake of nitrogen at $P/P_0 < 0.1$ reflects their limited microporosity. For the alkaline-treated ZSM-22 series samples, the nitrogen adsorption−desorption isotherms in the range of moderate to high relative pressures showed obvious hysteresis loops, as exhibited in Figure 4b, which indicates that alkaline treatment induced the appearance of mesopores,[38] consistent with TEM results. The nitrogen load at $P/P_0 = 0.99$ increased with the severity of alkaline treatment. In addition, the pore

https://doi.org/10.1021/acsomega.2c05478
ACS Omega 2023, 8, 14349−14364

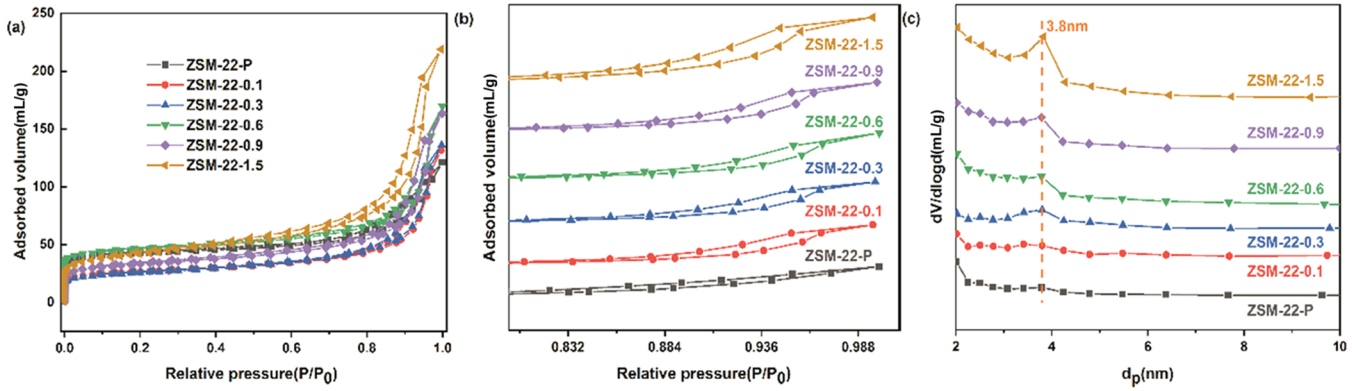

Figure 4. (a) N_2 adsorption and desorption isotherms, (b) hysteresis loops, and (c) pore size distributions of ZSM-22-P and ZSM-22-*x* series samples.

size distributions centered at 3.8 nm (slightly lower than the results from TEM images) of ZSM-22-P and ZSM-22-*x* series samples presented in Figure 4c also demonstrated the appearance of mesopores induced by alkaline treatment. Textural parameters of ZSM-22-P and ZSM-22-*x* series samples presented in Table 1 indicate that their external specific surface areas increased with the increase of alkaline aqueous concentration. In addition, the mesoporous volumes increased from 0.17 $mL{\cdot}g^{-1}$ (ZSM-22-P) to 0.21 $mL{\cdot}g^{-1}$ (ZSM-22-0.6) and 0.31 $mL{\cdot}g^{-1}$ (ZSM-22-1.5). Conversely, the micropore volumes of alkaline-treated zeolite samples decreased to different extents with the severity of alkaline treatment. In fact, the reduced microporosity of zeolites after alkaline treatment has been reported in other studies.[39−41] The most direct explanation for this phenomenon is that the debris removed from the framework during alkaline treatment integrated with the outer surface of the solid sample and then blocked the pore mouth. Considering that the removal of framework Si during alkaline treatment will inevitably affect neighboring framework Al and thus affect the acidity of ZSM-22 zeolite, it is necessary to study the effect of alkaline treatment on the acidity of ZSM-22 zeolite.

3.1.2. Acidity. Full NH_3-TPD profiles of ZSM-22-P and ZSM-22-*x* series samples are given in Figure 5. Apparently, all tested samples exhibited two desorption peaks, where the low-temperature peak was considered to be caused by the weak acid sites, while the high-temperature peak was generally believed to be induced by the desorption of ammonia adsorbed on the strong active sites.[42] For ZSM-22 zeolite, only its strong acid sites exert an influence on the skeletal isomerization reaction of 1-butene, so only high-temperature peaks were studied in this study. Compared with the ZSM-22-P sample, the high-temperature peak areas of ZSM-22-*x* series samples reduced sharply, as shown in Figure 5, indicating that alkaline treatment led to a decrease in the acid content of the ZSM-22-P sample. Figure 6a shows the IR spectra of the hydroxyl region of ZSM-22-P and ZSM-22-*x* series samples. With the severity of the alkaline treatment, the intensity of the band at 3735 cm^{-1}, attributed to isolated silanol located on the external surface of ZSM-22 zeolite,[43] also increased, corresponding to the increased external specific surface areas of ZSM-22-*x* series samples (Table 1). Analogous observations were also made in other studies.[43,44] Moreover, the bands at 3583 cm^{-1}, related to SiOHAl, *i.e.*, Brønsted acid sites,[43] also displayed different extents of changes. In order to quantitatively determine the effect of alkaline treatment on the amounts of Brønsted and

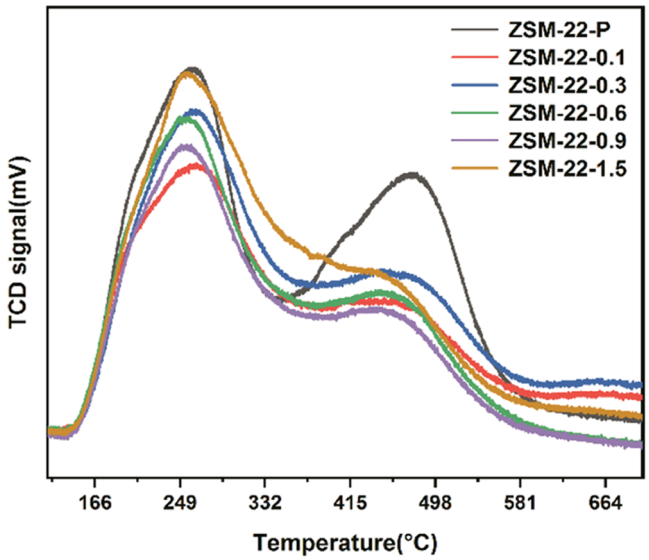

Figure 5. NH_3-TPD profiles of ZSM-22-P and ZSM-22-*x* series samples.

Lewis acids for ZSM-22-P, pyridine adsorption followed by infrared spectroscopy was implemented for ZSM-22-P and ZSM-22-*x* series samples. The spectra in the 1400−1600 cm^{-1} region are shown in Figure 6b, and the quantitative results of Py-IR are shown in Table 2. The peak at 1545 cm^{-1} is attributable to Brønsted acid sites, and the peak at 1454 cm^{-1} is related to Lewis acid sites.[45,46] Essentially, alkaline treatment resulted in the reduction of the Brønsted acid content and the simultaneous formation of Lewis acid sites. This phenomenon ensures that there is no significant change in the Si/Al ratio, as shown in Table 1, due to simultaneous desilication and dealumination during the process of ZSM-22 zeolite treatment with low NaOH aqueous concentration.

3.1.3. Evidence of the Coating Effect of Extra-Framework Al on the External Surface. The next question is how did the alkaline treatment decrease the amounts of Brønsted acid sites and increase the Lewis acid site contents of ZSM-22-P samples. To solve this problem, ZSM-22-*x* series samples were subjected to acid-washing treatment due to the dealumination effect of acid. The XRD patterns shown in Figure S1 indicate that ZSM-22-*x*-H series samples still present the pure TON phase. Interestingly, increased crystallinities of ZSM-22-0.6 and ZSM-22-0.9 samples were observed after the acid-washing

https://doi.org/10.1021/acsomega.2c05478
ACS Omega 2023, 8, 14349−14364

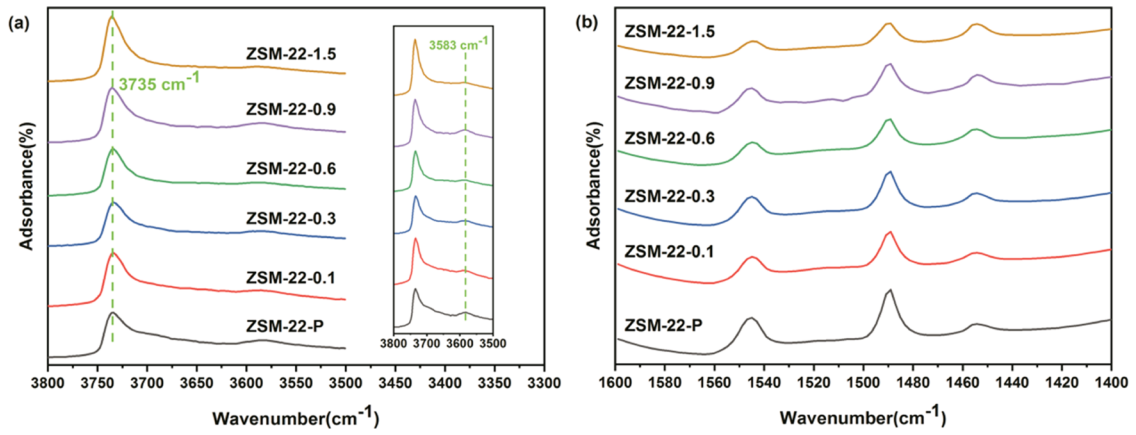

Figure 6. (a) IR spectra in the region of 3800−3500 cm^{-1} and (b) Py-IR spectra in the region of 1600−1400 cm^{-1} of ZSM-22-P and ZSM-22-*x* series samples.

Table 2. Acidity Properties of ZSM-22-P and ZSM-22-*x* Series Samples

	acid amounts in Py-IR (μmol·g^{-1})	
sample	Brønsted acid	Lewis acid
ZSM-22-P	555	102
ZSM-22-0.1	357	94
ZSM-22-0.3	418	123
ZSM-22-0.6	272	115
ZSM-22-0.9	358	174
ZSM-22-1.5	208	175

treatment (Figures 1 *vs* S1). A similar phenomenon was also observed for the Y zeolite after dealumination using ammonium fluorosilicate as the dealumination agent due to the removal of amorphous species.[47] As expected, the acid-washing treatment contributed to the restoration of the micropore volume of ZSM-22-*x* series samples with respect to the ZSM-22-P sample (Figure S2 and Table S1 *vs* Figure 4a and Table 1). In addition, the acid-washing treatment did not cause obvious changes in their morphologies (Figures S3 *vs* 2). According to the infrared spectra of ZSM-22-*x*-H series samples shown in Figure S4 and their quantitative results shown in Table S2, the acid-washing treatment caused a decrease of their Lewis acid site density and an increase in the number of Brønsted acid sites for ZSM-22-*x* series samples. These phenomena led us to conclude that the extra-framework Al generated during the alkaline treatment covered the partial Brønsted acid sites of the ZSM-22-P sample.

The external Lewis acid sites of ZSM-22 series samples were detected by infrared spectroscopy of adsorbed collidine. As shown in Figure 7, compared with ZSM-22-P samples, the peak intensities at 1639 cm^{-1}, related to the adsorption of collidine on the Lewis acid sites,[48] enhanced to varying degrees after the alkaline treatment. In contrast, the intensities of bands at 1639 cm^{-1} decreased for the acid-washed samples. We attributed this to the fact that a fraction of extra-framework Al species produced in the process of the alkaline treatment was accessible to collidine and most of them can be removed by the acid-washing treatment.

In order to further study the variation in the type and quantity of surface Al species after the alkaline treatment, typical ZSM-22 series samples were characterized by XPS. Figure 8 shows Al 2p XPS spectra of selected ZSM-22 series samples, and Table 3 lists the surface Al contents of selected

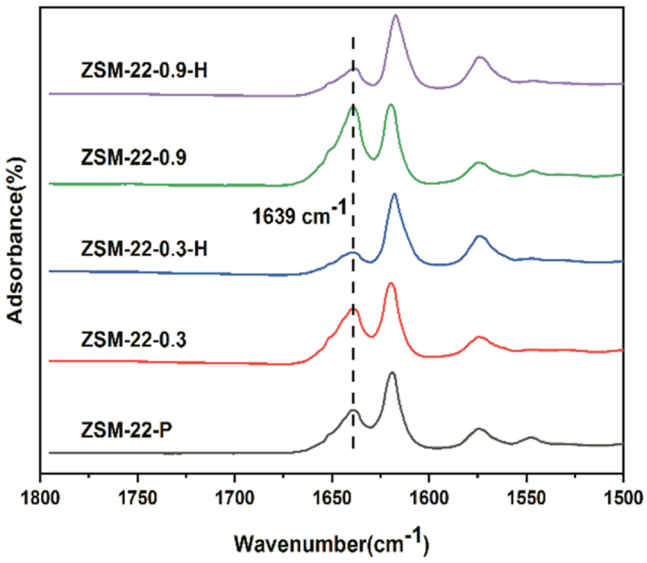

Figure 7. IR spectra of collidine adsorption in the region of 1800−1500 cm^{-1} of typical ZSM-22 series samples.

ZSM-22 series samples and the respective proportions of framework Al and extra-framework Al species on their surface. The alkaline treatment caused the enrichment of surface Al species, while acid-washing treatment removed Al species from the surface to some extent. Moreover, the Al 2p spectra of different samples were decomposed into two peaks. The decomposition peaks with binding energies of 75 and 74 eV, respectively, correspond to the framework Al[49] and extra-framework Al like $Al(OH)_3$ or AlOOH species.[50,51] Apparently, the amounts of extra-framework Al, *e.g.*, $Al(OH)_3$ or AlOOH species, increased after the alkaline treatment, while decreased contents of extra-framework Al species can be observed for the acid-washed samples. Combined with the infrared spectra of adsorbed pyridine and collidine, it can be confirmed that the alkaline treatment results in the occurrence of dealumination and then some of the removed framework Al like $Al(OH)_3$ or AlOOH species are redeposited on the external surface of ZSM-22-*x* series samples, which subsequently covers their partial external Brønsted acid sites.

3.1.4. Summary of Effects of Alkaline Treatment on ZSM-22 Zeolites. The attack of OH^- on the Si−O−Si bond in the zeolite framework caused by alkaline treatment frequently

https://doi.org/10.1021/acsomega.2c05478
ACS Omega 2023, 8, 14349−14364

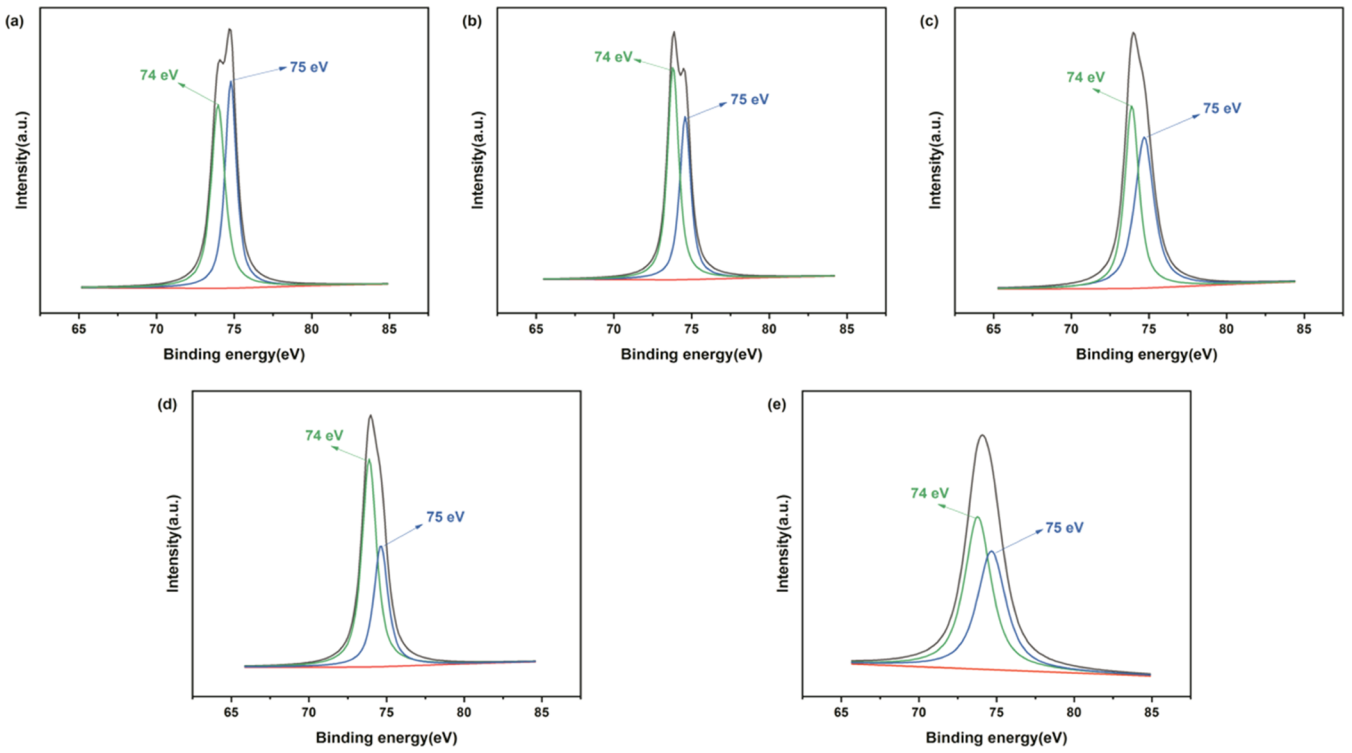

Figure 8. Al 2p XPS spectra of the typical ZSM-22 series samples: (a) ZSM-22-P, (b) ZSM-22-0.3, (c) ZSM-22-0.3-H, (d) ZSM-22-0.9, and (e) ZSM-22-0.9-H.

Table 3. Quantified Results of Al 2p XPS Spectra of the Typical ZSM-22 Series Samples

sample	surface Al content (%)	percentage of framework Al in surface content (%)	percentage of extra-framework Al in surface content (%)
ZSM-22-P	1.32	47.98	52.02
ZSM-22-0.3	1.67	42.83	57.17
ZSM-22-0.3-H	1.43	52.68	47.32
ZSM-22-0.9	2.47	36.10	63.90
ZSM-22-0.9-H	1.26	45.44	54.56

results in desilication.[52−54] Several factors affect the desilication efficiency, among which the Si/Al ratio of the parent zeolite is an important parameter.[55−57] A low Si/Al ratio inhibits the attack of OH^- ions on the framework Si, while high-density silicon tends to be overdissolved. Many research groups took advantage of this principle to prepare hierarchical zeolites[39,58,59] and hollow crystals.[60−62] In the process of desilication, in addition to framework Al, extra-framework Al also plays a certain protective role.[56] For example, some Al debri formed during desilication are redeposited on the external surface of zeolite,[63,64] which further form Al-rich layers and thus plug micropores.

Based on the previous characterization results and the above analysis, we proposed the following mechanisms of alkaline treatment and the subsequent acid-washing treatment. As shown in Scheme 1, after alkaline treatment, the framework Si in the nanorod-like ZSM-22 crystals was selectively removed to generate inter- and intracrystalline mesopores. However, the disordered propagation of some intracrystalline mesopores resulted in the fragmentation of ZSM-22-P zeolite crystals, which resulted in an increase in the external surface of the alkaline-treated samples. At the same time, in the process of alkali treatment, part of the extra-framework Al was deposited on the external surface of the crystals, covering part of the Brønsted acid sites and thus blocking their pore mouths. After the subsequent acid-washing treatment, the extra-framework Al on the external surface of ZSM-22 zeolite crystals was removed, and then the acidic sites on the external surface and micropore volumes were partially recovered.

Scheme 1. Schematic Representation of (a) ZSM-22-P, (b) ZSM-22-*x* Series, and (c) ZSM-22-*x*-H Series Samples

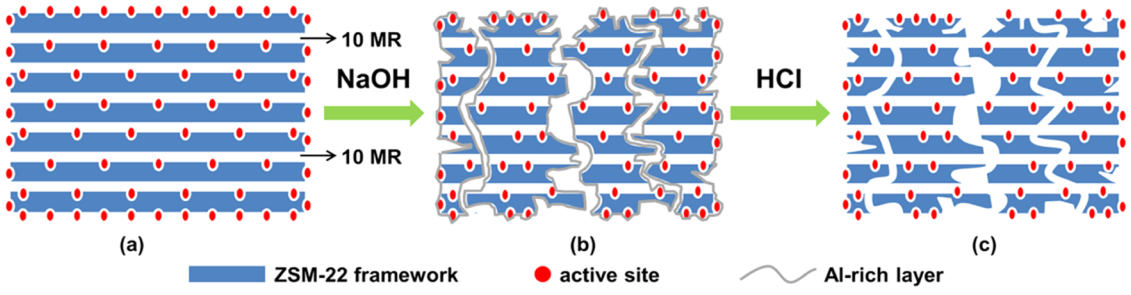

https://doi.org/10.1021/acsomega.2c05478
ACS Omega 2023, 8, 14349−14364

3.2. Catalytic Performances of ZSM-22-*x* and ZSM-22-*x*-H Series Samples. The 1-butene conversions of ZSM-22-P and ZSM-22-*x* series samples are shown in Figures 9 and S5a,

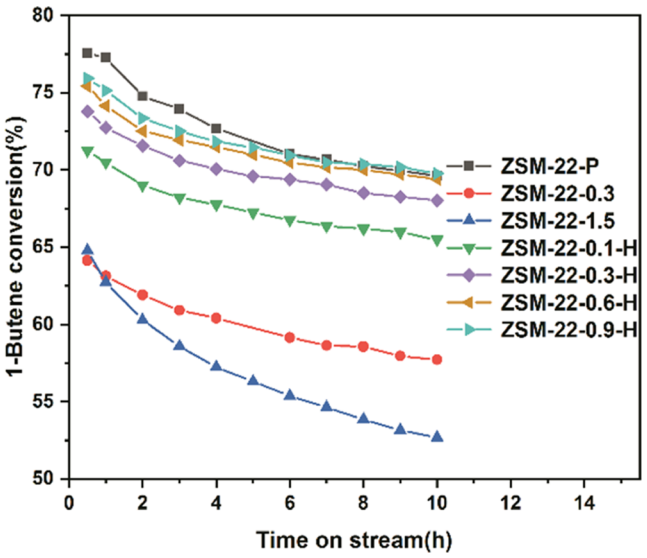

Figure 9. Results of 1-butene conversion of ZSM-22-P, ZSM-22-*x*, and ZSM-22-*x*-H series samples *vs* TOS in the skeletal isomerization of 1-butene to isobutene.

respectively. The 1-butene conversion of ZSM-22-P at 0.5 h was 78%, and its activity at 10 h was 70%. In contrast, the overall activities of ZSM-22-*x* series samples were significantly lower than those of ZSM-22-P samples during the reaction time of 10 h. It is generally considered that the activity of the zeolite catalyst, especially the initial activity, is related to its acid strength,[65,66] the accessibility of its acid sites,[67−69] the existence of Lewis acid sites,[18,70,71] and its acid content.[7,72] The NH_3-TPD results shown in Figure 5 showed that the acid strength of ZSM-22-*x* series samples was similar to that of the ZSM-22-P sample. Therefore, the influence of acid strength of ZSM-22-*x* series samples on their activities can be excluded in this study. According to SEM, TEM, and N_2 physical adsorption results, compared with the ZSM-22-P sample, ZSM-22-*x* series samples possessed higher external specific surface areas and mesopore volumes. In principle, 1-butene molecules were more easily accessible to their acid sites and they should have higher activities, but it was not the case with the experimental results, and so the influence of increased mesopore volumes and external specific surface areas in ZSM-22-*x* series samples can be ruled out. In addition, the high contents of extra-framework Al in ZSM-22-*x* series samples were also noteworthy. It has been reported that the spatial proximity between extra-framework Al and framework Al of zeolite will cause a partial transfer of electrons from acidic OH bonds to extra-framework Al species, thus increasing the acid strength of zeolite by reducing the strength of OH bonds.[71,73] As mentioned above, the activities of ZSM-22-*x* series samples did not reflect the effect of their acid strength, indicating that there were no synergistic effects between the extra-framework Al produced by desilication and the pristine Brønsted acid sites. According to the results shown in Scheme 1, extra-framework Al only served to cover the outer acidic sites of ZSM-22-*x* series samples. Therefore, it was assumed that the effect of alkaline treatment on the activity of the ZSM-22-P sample was mainly attributed to the reduced amounts of Brønsted acid sites (Figure 6b and Table 2). After evaluating the activities of ZSM-22-*x*-H series samples under the same conditions, it was observed that the activities of ZSM-22-*x*-H series samples were higher than those of the corresponding alkaline-treated samples (Figures 9 and S5a), which further confirmed the influence of the Brønsted acid contents of ZSM-22 zeolite on its activity.

It is generally believed that there are three main reaction pathways involved in the transformation of 1-butene into isobutene: bimolecular reaction mechanism, monomolecular reaction mechanism, and pseudo-monomolecular reaction mechanism,[15,24,74−76] as shown in Scheme 2. In the bimolecular reaction mechanism, two 1-butene molecules dimerize to form C_8 molecules such as dimethylhexene (DMH) and trimethylpentene (TMP), and then they undergo isomerization and cracking reactions to form isobutene. In addition, C_8 molecules also further crack to produce byproducts such as propylene and pentene. In terms of monomolecular and pseudomonomolecular mechanisms, 1-butene can be selectively converted to isobutene. According to the above-mentioned reaction mechanisms, we emphatically analyzed the yields of isobutene and propylene to study the effect of alkaline treatment on the catalytic performances of ZSM-22 zeolite. As shown in Figures 10 and S5, the overall isobutene yields of ZSM-22-*x* series samples were about 40%. The isobutene yield of the ZSM-22-P sample was 29% at 0.5 h and 38% at 10 h. Conversely, the propylene yields of ZSM-22-*x* series samples were all much lower than that of the ZSM-22-

Scheme 2. Simplified Reaction Mechanisms of 1-Butene Skeletal Isomerization[a]

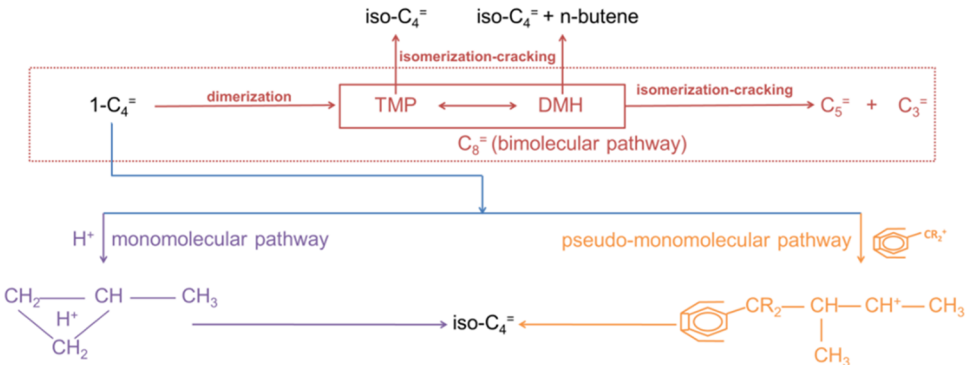

[a]TMP = trimethylpentene; DMH = dimethylhexene.

https://doi.org/10.1021/acsomega.2c05478
ACS Omega 2023, 8, 14349−14364

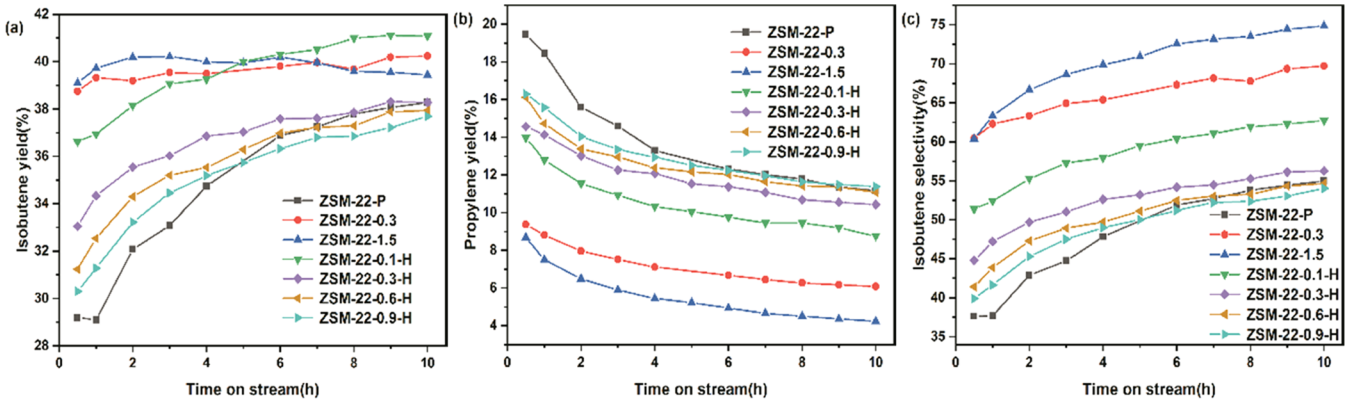

Figure 10. Results of (a) isobutene yield, (b) propylene yield, and (c) isobutene selectivity of ZSM-22-P, ZSM-22-*x*, and ZSM-22-*x*-H series samples *vs* TOS in the skeletal isomerization of 1-butene to isobutene.

P sample. As a result, the isobutene selectivities of ZSM-22-*x* series samples were higher than that of the ZSM-22-P sample. These results showed that the overall catalytic performances of the alkaline-treated ZSM-22 series zeolites were better than that of ZSM-22-P zeolite. Moreover, information related to the catalytic performances of ZSM-22 zeolite in the 1-butene skeletal isomerization reaction at a reaction temperature of 400 °C in other studies is presented in Table 4. Clearly, except that

Table 4. Comparison of Catalytic Properties of ZSM-22 Zeolites Evaluated at 400 °C

sample	reaction pressure	WHSV (h^{-1})	isobutene yield (%)	isobutene selectivity (%)	refs
1	0.5 atm	150	<30	80−90	28
2	0.6 atm	200	<30	70−85	29
3	0.5 atm	150	<37.5	<70	30
4	0.5 atm	44	<37.5		74
5	atmospheric pressure	14	*ca.* 40	*ca.* 60−75	in this study[a]

[a]Alkaline-treated ZSM-22 series samples.

the isobutene selectivities of samples 1 and 2 were higher than those of ZSM-22-*x* series samples, the overall catalytic performances of samples studied by other groups were lower than those of the ZSM-22-*x* series samples in this study. It is clear that the space velocities used in other studies were higher than that applied in this study, and their reaction pressures were lower than the atmospheric pressure. Considering that a higher reactant pressure and lower space velocity easily lead to the dimerization reaction of 1-butene and then reduce the yield and selectivity of isobutene,[28] ZSM-22-*x* series samples showed relatively better catalytic properties under the reaction conditions that were unfavorable to gain high isobutene selectivity with respect to the catalytic performances of ZSM-22 zeolites obtained in other studies at a reaction temperature of 400 °C.

In order to find the reason for the high isobutene yields and selectivities of ZSM-22-*x* series samples, we compared the isobutene and propylene yields between ZSM-22-*x* and ZSM-22-*x*-H series samples (Figures 10 and S5). It was noticed that the higher Brønsted acid contents caused a decrease in the isobutene yield and an increase in the propylene yield and thus the decrease in the isobutene selectivity. Therefore, combined with the results of NH_3-TPD, Py-IR, and activity, we concluded that the improved isobutene yields and selectivities of ZSM-22-*x* series samples are derived from their reduced Brønsted acid contents.

3.3. Relationship between the Location of Carbon Deposition and Catalytic Performances of ZSM-22 Series Zeolites. In the acid catalytic reactions of hydrocarbon transformation, zeolite catalysts are often confronted with the deactivation phenomena originating from the formation of coke.[77] Because carbon deposition is precisely caused by a series of acid-catalyzed side reactions, its properties can conversely reflect some characteristics of the acidic sites of zeolite catalysts. In an effort to gain a better understanding of the factors affecting the catalytic performances of ZSM-22 series zeolites, it is necessary to study the properties of the carbon deposition formed during the reaction process.

Figure 11a,b exhibits the coke contents of used ZSM-22-*x* and ZSM-22-*x*-H series samples, respectively. The results showed that the contents of coke deposited on used ZSM-22-*x* series samples basically remained in the range of 7−9%, except for the ZSM-22-0.3 sample. The acid-washing treatment did not significantly affect their coke contents. However, it is worth noting that the temperatures corresponding to the maximum change rate of weight loss were overall lower for ZSM-22-*x* series samples with respect to ZSM-22-P and ZSM-22-*x*-H series samples, as indicated by the differential thermogravimetric curves shown in Figure 11c,d. This phenomenon is attributed, on the one hand, to the property differences of carbon deposition on the two series of samples,[78,79] and on the other hand, to the location of carbon deposition.[80]

To shed light on the chemical nature of the deactivated species, we utilized Raman spectroscopy to characterize the used ZSM-22-*x* and ZSM-22-*x*-H series samples. As shown in Figure 12, all of the coked samples exhibited peaks around 1170−1180 and 1390−1400 cm^{-1} corresponding to the C−H bond vibration of coke species.[81,82] Additional bands at 1605−1610 cm^{-1} related to conjugated olefins species[83] were also observed. Obviously, the relative intensities of these bands were similar, which emphasizes the comparable coke properties for the coked ZSM-22-*x* and ZSM-22-*x*-H series samples. Therefore, it was speculated that the locations of carbon deposition on the surfaces of ZSM-22-*x* and ZSM-22-*x*-H series samples were different. In order to distinguish the location of coke deposition on each sample, the TG/MS-TPO instrument was used. Figure 13 presents the TPO profiles of the spent ZSM-22-*x* and ZSM-22-*x*-H series samples, where two peaks corresponding to two types of cokes, coke types I and II, were distinguished. Moreover, significant differences

https://doi.org/10.1021/acsomega.2c05478
ACS Omega 2023, 8, 14349−14364

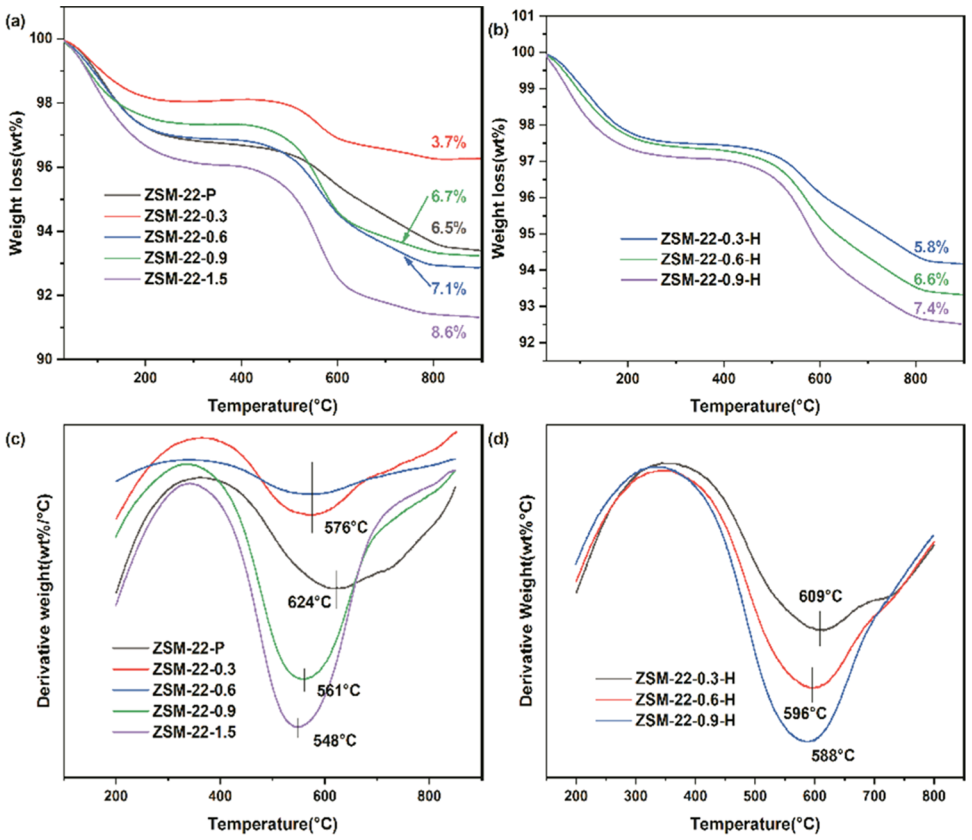

Figure 11. TG and derivative thermogravimetry (DTG) curves of the used (a, c) ZSM-22-*x* and (b, d) ZSM-22-*x*-H series samples after 10 h of TOS obtained in an air atmosphere.

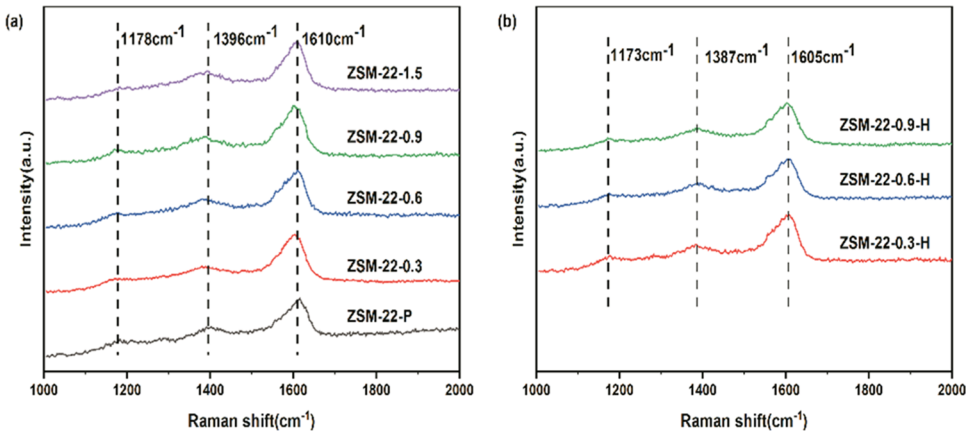

Figure 12. Raman spectra of (a) ZSM-22-*x* and (b) ZSM-22-*x*-H series samples.

were observed in the relative amounts between coke types I and II. Clearly, the content of coke type I for ZSM-22-*x* series samples was higher than that for ZSM-22-P and ZSM-22-*x*-H series samples, while the reverse trend was observed for the coke type II content (Figure 13 and Table S3). It is widely recognized that the combustion of coke type II occurs at higher temperatures due to the constraints imposed by zeolite micropores. Naturally, coke type I is located on the external surface.[80] Therefore, it was expected that compared with ZSM-22-P and ZSM-22-*x*-H series samples, the effective active sites for the isomerization reaction of ZSM-22-*x* series samples were mainly located on the outer surface. Together with the results of catalytic performances, we can further confirm that the improved catalytic performances of ZSM-22-*x* series samples were attributed to the fact that the extra-framework Al extracted from the framework during the alkaline treatment partially covered the external Brønsted acid sites.

3.4. Relationship between the Amounts of External Acid Sites and Catalytic Performances of ZSM-22 Series Zeolites. The above results suggest that the catalytic performances of ZSM-22 zeolite can be improved by reducing its external Brønsted acid site density. In order to gain deeper insights into the relationship between the isobutene yield and selectivity and external acid site density of ZSM-22-P samples, and to further elaborate the effect of alkaline treatment on the reduction of the available outer acid site density of ZSM-22-P

https://doi.org/10.1021/acsomega.2c05478
ACS Omega 2023, 8, 14349−14364

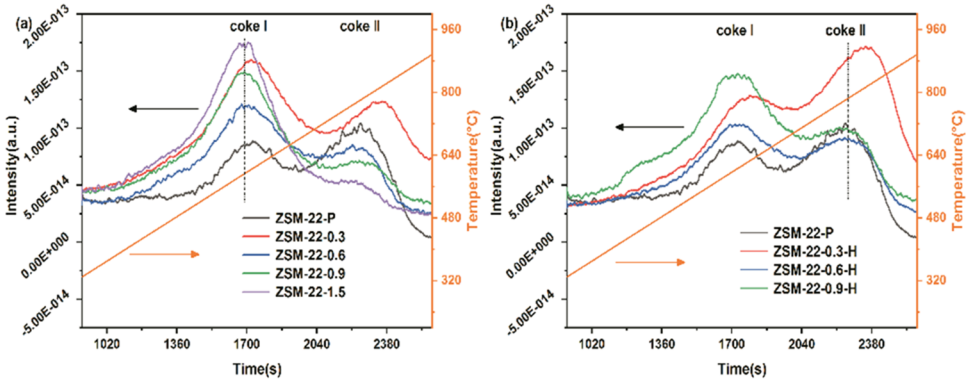

Figure 13. Signal curves of the released CO_2 (m/z = 44) of the coke deposited on the used (a) ZSM-22-x and (b) ZSM-22-x-H series samples during oxidation.

Scheme 3. Modification of External Acid Sites of ZSM-22 Zeolite

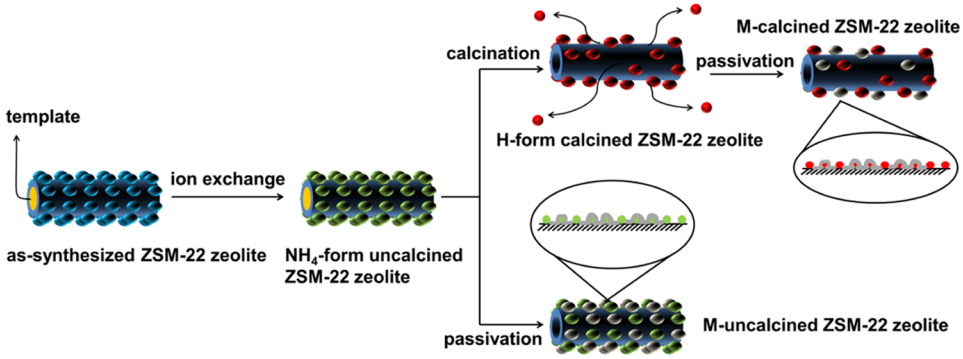

sample, we explored the dependence of its external acid sites and its catalytic performances according to the experimental protocols shown in Scheme 3.

Because the template agent was filled in its microporous channels (Figure S6 and Table S4) and retained intact under experimental conditions (Figure S7), it can be assumed that its active sites were located only on its external surface for the NH_4-form uncalcined ZSM-22 zeolite. Furthermore, considering that the calcination treatment can reduce the number of acid sites to a certain extent in the case of zeolite,[84] the NH_4-form uncalcined ZSM-22 sample was calcined to obtain samples with fewer external acid sites, *i.e.*, H-form calcined ZSM-22 sample. In addition, as the size of tetraethyl orthosilicate (TEOS) (10.3 Å[85]) is much larger than the pore size of ZSM-22 zeolite (4.6 × 5.7 Å^2, 10MR),[86] the chemical liquid deposition method of TEOS could only passivate the external acid sites of zeolite.[35] Therefore, ZSM-22 zeolite samples with fewer external acidic sites (M-calcined ZSM-22 and M-uncalcined ZSM-22) can be further prepared by chemical liquid deposition.

The catalytic properties of the above-mentioned four samples were all evaluated (because the NH_4-form uncalcined ZSM-22 zeolite was pretreated for 30 min in a N_2 atmosphere at 400 °C before reaction (see Section 2.5) and the NH_4-form zeolite will undergo a deamination reaction and then change into the H-form zeolite at 400 °C,[87−89] NH_4-form uncalcined ZSM-22 zeolite can be directly used to catalyze the reaction). As expected, their activities at 10 h followed the sequence as follows: NH_4-form uncalcined ZSM-22 > H-form calcined ZSM-22 = M-uncalcined ZSM-22 > M-calcined ZSM-22 (Figure 14). However, their isobutene yields and isobutene

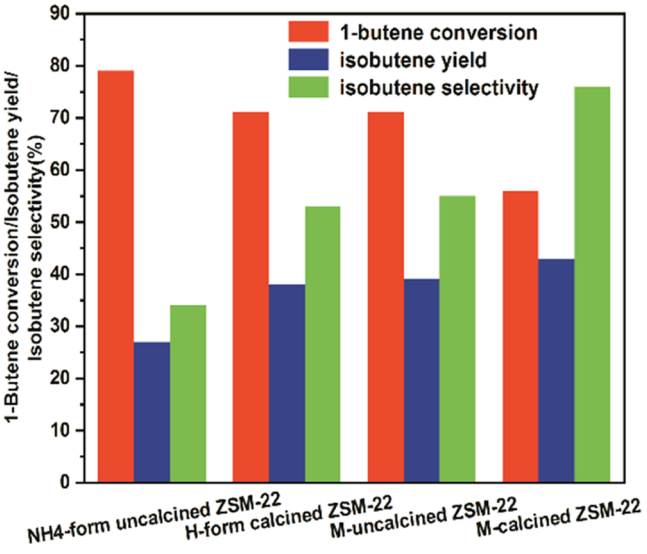

Figure 14. Comparison of 1-butene conversion, isobutene yield, and isobutene selectivity at 10 h of the NH_4-form uncalcined ZSM-22, H-form calcined ZSM-22, M-uncalcined ZSM-22, and M-calcined ZSM-22.

selectivities were in the opposite order. These results indicated that the catalytic performances of ZSM-22 zeolite improved with the decrease of the amount of its external acidic sites, which indirectly confirms the effect of alkaline treatment on the external acidic sites of ZSM-22 zeolite. In addition, the external acid sites of ZSM-22-P, ZSM-22-0.9, and ZSM-22-0.9-H samples were also passivated by TEOS, respectively. Their

https://doi.org/10.1021/acsomega.2c05478
ACS Omega 2023, 8, 14349−14364

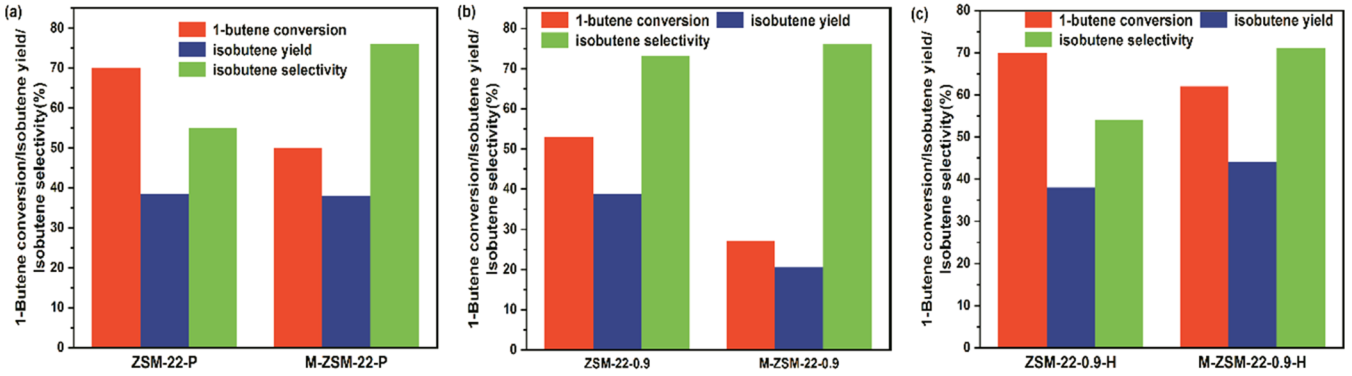

Figure 15. Comparison of 1-butene conversion, isobutene yield, and isobutene selectivity at 10 h of the selected samples before and after partial passivation of external acid sites: (a) ZSM-22-P and M−ZSM-22-P, (b) ZSM-22-0.9 and M−ZSM-22-0.9, and (c) ZSM-22-0.9-H and M−ZSM-22-0.9-H.

Scheme 4. Reason for the Improvement in Isobutene Selectivity of ZSM-22 Zeolite by Alkaline Treatment

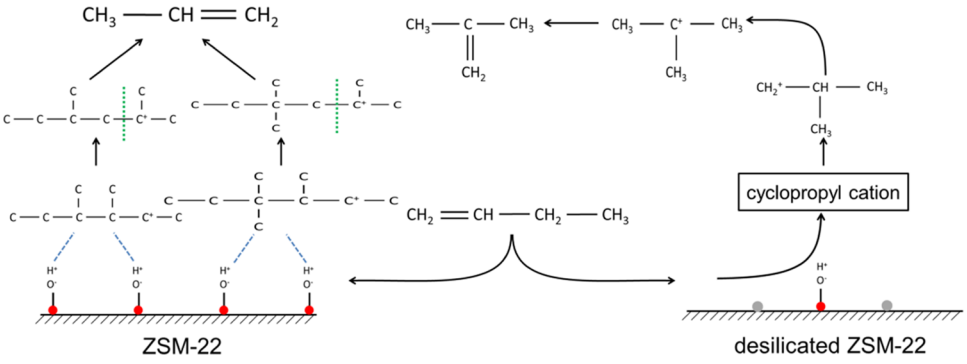

respective catalytic results at 10 h are shown in Figure 15. Similarly, their activities decreased with respect to their respective unpassivated samples, indicating that some of the external acid sites were successfully passivated by TEOS. All of their selectivities for isobutene increased after partial passivation of their external active sites. Moreover, the isobutene yield of the M−ZSM-22-0.9-H sample higher than that the ZSM-22-0.9-H sample, but the isobutene yield of the M−ZSM-22-0.9 sample was lower than that of the ZSM-22-0.9 sample. These phenomena confirmed again that the improved catalytic performance of ZSM-22 zeolite originates from its decreased external acidity, but excessively low contents of external acid sites will result in its lower isobutene yield. These results also indirectly demonstrated that the enhanced catalytic performances of ZSM-22-*x* series samples were caused by the partial coverage of the external Brønsted acid sites by redeposited extra-framework Al in the process of alkaline treatment.

3.5. Essential Reason for the Improved Catalytic Performances of ZSM-22-*x* Series Zeolites. As shown in Scheme 2, two types of reaction mechanisms lead to the high isobutene selectivity in the skeletal isomerization reaction of 1-butene: (i) a pseudomonomolecular mechanism (alkylaromatic tertiary carbenium ion acting as the active site) and (ii) a monomolecular mechanism (proton acting as the active site). However, according to the results shown in Figures 11 and 12, the amounts and properties of coke deposited on ZSM-22-P and ZSM-22-*x* series samples were similar. In addition, as shown in Figure S8, the selectivity of isobutene was dependent only on the contact time between 1-butene and acid sites and is not affected by the resulting carbon deposition. Therefore, the main reaction mechanism resulting in high isobutene selectivity is the monomolecular reaction mechanism.

In this study, due to the formation of an Al-rich layer in the desilication process, the acid sites on the outer surface of ZSM-22 zeolite were partially covered (see Scheme 1). This phenomenon led to a decrease in its external acid sites. Figure 10 shows that the propylene yield of the parent ZSM-22 zeolite is 5−7% higher than those of the alkaline-treated ZSM-22 series samples under similar isobutene yields. It was reported that the closer the distance between the acid sites, the more conducive it is to the occurrence of dimerization reaction[90,91] and then the formation of propylene and other byproducts by the subsequent cracking reaction. Therefore, we proposed the following mechanism for the effect of alkaline treatment on catalytic performances of ZSM-22 zeolite. As shown in Scheme 4, due to the abundant acidic sites distributed on the external surface of the parent ZSM-22 zeolite, the adjacent protonated 1-butene molecules are prone to dimerize into C_8 molecules, which are further isomerized and cracked into propylene and other byproducts, thereby reducing the yield and selectivity of isobutene. For the alkaline-treated ZSM-22 zeolites, the partial coverage of their external acidic sites resulted in a greater distance among a part of the effective acid sites, which induced the occurrence of the selective skeletal isomerization of 1-butene by the direct interaction of individual 1-butene molecules with single active sites (*i.e.*, the monomolecular pathway). Therefore, the key to improve the catalytic performances of ZSM-22 zeolite in the skeletal isomerization reaction of 1-butene is the proper amount of external acid sites.

https://doi.org/10.1021/acsomega.2c05478
ACS Omega 2023, 8, 14349−14364

4. CONCLUSIONS

By treating the parent ZSM-22 zeolite with different concentrations of alkaline aqueous solution, it was found that the alkaline solution could cause partial dealumination, and then the extracted framework Al debris was redeposited on the outer surface, thus reducing the Brønsted acid site density. The subsequent acid-washing treatment can effectively remove the Al debris. Simultaneously, the amounts of Brønsted acid sites showed an increasing trend. After alkaline-treated samples and acid-treated samples were respectively applied in the skeletal isomerization reaction of 1-butene, the catalytic performances of the alkaline-treated samples were found to be significantly improved, while the isobutene yield and selectivity decreased sharply for subsequent acid-washed samples. By evaluating the coke distribution of coked samples, it was found that the coke was mainly deposited on the external surface of the alkaline-treated ZSM-22 zeolite. Moreover, the phenomenon of a lower content of external acidic sites of ZSM-22 zeolites leading to their higher catalytic performances was observed by partially passivating their external acid sites. The overall results of our work suggest that the reason for the enhanced catalytic properties of ZSM-22 zeolite is ascribed to the monomolecular reaction of 1-butene over external diluted acidic sites. The conclusion obtained is expected to provide a direction to improve the catalytic performance of other 10-ring channel zeolites in the skeletal isomerization of 1-butene.

■ ASSOCIATED CONTENT

Supporting Information

The Supporting Information is available free of charge at https://pubs.acs.org/doi/10.1021/acsomega.2c05478.

XRD patterns of ZSM-22-*x*-H series samples (Figure S1); N_2 adsorption and desorption isotherms of ZSM-22-*x*-H series samples (Figure S2); textural properties of ZSM-22-*x*-H series samples (Table S1); SEM images of ZSM-22-*x*-H series samples (Figure S3); Py-IR spectra of ZSM-22-*x*-H series samples (Figure S4); numbers of Brønsted acid sites and Lewis acid sites of ZSM-22-*x*-H series samples (Table S2); results of 1-butene conversion, isobutene yield, propylene yield, and isobutene selectivity of ZSM-22-*x* series samples *vs* TOS in the skeletal isomerization reaction of 1-butene to isobutene (Figure S5); peak areas and amounts of released CO_2 corresponding to coke I and coke II of the used ZSM-22-*x* and ZSM-22-*x*-H series samples (Table S3); N_2 adsorption and desorption isotherms of the NH_4-form uncalcined ZSM-22 sample (Figure S6); textural properties of the NH_4-form uncalcined ZSM-22 zeolite (Table S4); TGA curves of NH_4-form uncalcined ZSM-22 before and after reaction and signal curves of the released products of fresh NH_4-form uncalcined ZSM-22 sample in a helium atmosphere (Figure S7); results of isobutene selectivity *vs* TOS at 400 °C and 7 or 28 h^{-1} in 1-butene skeletal isomerization over ZSM-22-P and ZSM-22-0.9 (Figure S8) (PDF)

■ AUTHOR INFORMATION

Corresponding Author

Yunfeng Hu − *Provincial Key Laboratory of Oil & Gas Chemical Technology, College of Chemistry and Chemical Engineering, Northeast Petroleum University, Daqing 163318, P. R. China;* orcid.org/0000-0003-4827-9031; Email: huyunfeng@nepu.edu.cn

Authors

Guoliang Wu − *Provincial Key Laboratory of Oil & Gas Chemical Technology, College of Chemistry and Chemical Engineering, Northeast Petroleum University, Daqing 163318, P. R. China*

Qiang Bao − *Provincial Key Laboratory of Oil & Gas Chemical Technology, College of Chemistry and Chemical Engineering, Northeast Petroleum University, Daqing 163318, P. R. China;* orcid.org/0000-0001-8012-5425

Jian Zhang − *Provincial Key Laboratory of Oil & Gas Chemical Technology, College of Chemistry and Chemical Engineering, Northeast Petroleum University, Daqing 163318, P. R. China*

Junping Ge − *Provincial Key Laboratory of Oil & Gas Chemical Technology, College of Chemistry and Chemical Engineering, Northeast Petroleum University, Daqing 163318, P. R. China*

Complete contact information is available at: https://pubs.acs.org/10.1021/acsomega.2c05478

Notes

The authors declare no competing financial interest.

■ ACKNOWLEDGMENTS

This study was funded by the PetroChina Innovation Foundation, China (2012D5006-0403), PetroChina Technology Development (2014A-2610), and the National Natural Science Foundation of China (51702044).

■ REFERENCES

(1) Al-Megren, H. A.; Barbieri, G.; Mirabelli, I.; Brunetti, A.; Drioli, E.; Al-Kinany, M. C. Direct conversion of n-butane to isobutene in a membrane reactor: thermodynamic analysis. *Ind. Eng. Chem. Res.* **2013**, *52*, 10380−10386.

(2) Nuyken, O.; Vierle, M.; Kühn, F. E.; Zhang, Y. Solvent-ligated transition metal complexes as initiators for the polymerization of isobutene. *Macromol. Symp.* **2006**, *236*, 69−77.

(3) Poźniczek, J.; Małecka-Lubańska, A.; Micek-Ilnicka, A.; Bielański, A. Gas phase hydration of isobutene to tert-butyl alcohol on $H_4SiW_{12}O_{40}$ as the catalyst. *Appl. Catal., A* **1999**, *176*, 101−109.

(4) Wang, G.; Cai, G. Cooperative catalytic effects between Brønsted and Lewis acid sites and kinetics for production of methyl methacrylate on SO_4^{2-}/TiO_2-SiO_2. *Chem. Eng. Sci.* **2021**, *229*, No. 116165.

(5) Madon, R. J.; Koermer, G. S.; Deeba, M.; Yau, K. Y. Fluid Catalytic Cracking Process for Increased Formation of Isobutylene and Isoamylenes. U.S. Patent US05,243,121A, 1993.

(6) Zhu, Q.; Wang, G.; Liu, J.; Su, L.; Li, C. Effect of Sn on isobutane dehydrogenation performance of Ni/SiO_2 Catalyst: adsorption modes and adsorption energies of isobutane and isobutene. *ACS Appl. Mater. Interfaces* **2017**, *9*, 30711−30721.

(7) Jo, D.; Lee, K.; Park, G. T.; Hong, S. B. Acid site density effects in zeolite-catalyzed 1-butene skeletal isomerization. *J. Catal.* **2016**, *335*, 58−61.

(8) Mirabelli, I. Dehydroisomerization of n-Butane to Isobutene. In *Encyclopedia of Membranes*, 1st ed.; Drioli, E.; Giorno, L., Eds.; Springer Berlin Heidelberg: Heidelberg, 2015; pp 1−3.

(9) Sahebdelfar, S.; Bijani, P. M.; Saeedizad, M.; Zangeneh, F. T.; Ganji, K. Modeling of adiabatic moving-bed reactor for dehydrogenation of isobutane to isobutene. *Appl. Catal., A* **2011**, *395*, 107−113.

(10) Houžvička, J.; Ponec, V. Skeletal isomerisation of n-butene on phosphorus containing catalysts. *Appl. Catal., A* **1996**, *145*, 95−109.

(11) Gao, S.; Moffat, J. B. Isomerization of 1-butene on supported and unsupported metal-oxygen cluster compounds (heteropoly oxometalates). *Catal. Lett.* **1996**, *42*, 105−111.
(12) Seo, G.; Kim, N.-H.; Lee, Y.-H.; Kim, J.-H. Influence of the fluorine loading level on the skeletal isomerization of 1-butene over fluorine-modified alumina. *Catal. Lett.* **1998**, *51*, 101−107.
(13) Cheng, Z. X.; Ponec, V. On the problems of the mechanism of the skeletal isomerization of n-butene. *Catal. Lett.* **1994**, *27*, 113−117.
(14) Seo, G.; Kim, N.-H.; Lee, Y.-H.; Kim, J.-H. Skeletal isomerization of 1-butene over mesoporous materials. *Catal. Lett.* **1999**, *57*, 209−215.
(15) van Donk, S.; Bitter, J. H.; de Jong, K. P. Deactivation of solid acid catalysts for butene skeletal isomerisation: on the beneficial and harmful effects of carbonaceous deposits. *Appl. Catal., A* **2001**, *212*, 97−116.
(16) Jae, J.; Tompsett, G. A.; Foster, A. J.; Hammond, K. D.; Auerbach, S. M.; Lobo, R. F.; Huber, G. W. Investigation into the shape selectivity of zeolite catalysts for biomass conversion. *J. Catal.* **2011**, *279*, 257−268.
(17) Houžvička, J.; Hansildaar, S.; Ponec, V. The shape selectivity in the skeletal isomerisation of n -butene to isobutene. *J. Catal.* **1997**, *167*, 273−278.
(18) Wu, G.; Hu, Y.; Bao, Q.; Zhang, J.; Wang, Y.; Ge, J.; Xu, M. The study of ferrierite zeolite synthesized by using silica sol modified by HCl as silica source for the skeletal isomerization reaction of 1-butene. *React. Kinet., Mech. Catal.* **2021**, *133*, 309−325.
(19) Lee, Y.; Park, M. B.; Kim, P. S.; Vicente, A.; Fernandez, C.; Nam, I. S.; Hong, S. B. Synthesis and catalytic behavior of ferrierite zeolite nanoneedles. *ACS Catal.* **2013**, *3*, 617−621.
(20) Seo, G.; Jeong, H. S.; Hong, S. B.; Uh, Y. S. Skeletal isomerization of 1-butene over ferrierite and ZSM-5 zeolites: influence of zeolite acidity. *Catal. Lett.* **1996**, *36*, 249−253.
(21) Xu, W. Q.; Yin, Y. G.; Suib, S. L.; O'young, C. L. Selective conversion of n-butene to isobutylene at extremely high space velocities on ZSM-23 Zeolites. *J. Catal.* **1994**, *150*, 34−45.
(22) Yang, S. M.; Guo, D. H.; Lin, J. S.; Wang, G. T. 1-Butene Conversion over SAPO-11 and MeAPO-11. In *Zeolites and Related Microporous Malerials: Stale of the Art*, 1st ed.; Weiikamp, J.; Karge, H. G.; Pfeifer, H.; Höldcrich, W., Eds.; Elsevier Science BV: Amsterdam, 1994; pp 1677−1684.
(23) Liu, L.; Zhou, F.; Qiao, K.; Liu, Z. Study on skeletal isomerization of n-butenes into isobutene on molecular sieve with 10 MR pore structures. *Pet. Process. Petrochem.* **2013**, *44*, 55−58.
(24) Asensi, M. A.; Martinez, A. Selective isomerization of n-butenes to isobutene on high Si/Al ratio ferrierite in the absence of coke deposits: implications on the reaction mechanism. *Appl. Catal., A* **1999**, *183*, 155−165.
(25) Hu, H. Q.; Ke, M.; Zhang, K.; Liu, Q.; Yu, P.; Liu, Y.; Li, C. C.; Liu, W. Designing ferrierite-based catalysts with improved properties for skeletal isomerization of n-butene to isobutene. *RSC Adv.* **2017**, *7*, 31535−31543.
(26) Dai, H.; Lee, C.; Liu, W.; Yang, T.; Claret, J.; Zou, X.; Dauenhauer, P. J.; Li, X.; Rimer, J. D. Enhanced selectivity and stability of finned ferrierite catalysts in butene isomerization. *Angew. Chem.* **2022**, *134*, No. e202113077.
(27) Xu, Q.; Yang, W.; Chen, Z.; Ye, Y.; Luo, Y.; Street, J.; Zhou, H.; Xu, C. Formation and regeneration of shape-selective ZSM-35 catalysts for n-butene skeletal isomerization to isobutene. *ACS Omega* **2018**, *3*, 8202−8211.
(28) Byggningsbacka, R.; Kumar, N.; Lindfors, L. E. Comparative study of the catalytic properties of ZSM-22 and ZSM-35 ferrierite zeolites in the skeletal isomerization of 1-butene. *J. Catal.* **1998**, *178*, 611−620.
(29) Byggningsbacka, R.; Kumar, N.; Lindfors, L. E. Comparison of the catalytic properties of Al-ZSM-22 and Fe-ZSM-22 in the skeletal isomerization of 1-butene. *Catal. Lett.* **1999**, *58*, 231−234.
(30) Byggningsbacka, R.; Lindfors, L. E.; Kumar, N. Catalytic activity of ZSM-22 zeolites in the skeletal isomerization reaction of 1-butene. *Ind. Eng. Chem. Res.* **1997**, *36*, 2990−2995.
(31) Baeck, S. H.; Lee, W. Y. Skeletal isomerization of 1-butene to isobutene over Mg-ZSM-22. *Appl. Catal., A* **1997**, *164*, 291−301.
(32) Asensi, M. A.; Corma, A.; Martínez, A.; Derewinski, M.; Krysciak, J.; Tamhankar, S. S. Isomorphous substitution in ZSM-22 zeolite. The role of zeolite acidity and crystal size during the skeletal isomerization of n-butene. *Appl. Catal., A* **1998**, *174*, 163−175.
(33) Baeck, S. H.; Lee, W. Y. Dealumination of Mg-ZSM-22 and its use in the skeletal isomerization of 1-butene to isobutene. *Appl. Catal., A* **1998**, *168*, 171−177.
(34) Baeck, S. H.; Lee, K. M.; Lee, W. Y. Skeletal isomerization of 1-butene into isobutene over Mg-ZSM-22 modified by the deposition of silicon alkoxide. *Catal. Lett.* **1998**, *52*, 221−225.
(35) Zheng, S.; Heydenrych, H. R.; Jentys, A.; Lercher, J. A. Influence of surface modification on the acid site distribution of HZSM-5. *J. Phys. Chem. B* **2002**, *106*, 9552−9558.
(36) Čejka, J.; Wichterlová, B.; Sarv, P. Extent of monomolecular and bimolecular mechanism in n-butene skeletal isomerization to isobutene over molecular sieves. *Appl. Catal., A* **1999**, *179*, 217−222.
(37) Ahoba-Sam, C.; Erichsen, M. W.; Olsbye, U. Ethene and butene oligomerization over isostructural H-SAPO-5 and H-SSZ-24: kinetics and mechanism. *Chin. J. Catal.* **2019**, *40*, 1766−1777.
(38) Thommes, M.; Kaneko, K.; Neimark, A. V.; Olivier, J. P.; Rodriguez-Reinoso, F.; Rouquerol, J.; Sing, K. S. W. Physisorption of gases, with special reference to the evaluation of surface area and pore size distribution (IUPAC Technical Report). *Pure Appl. Chem.* **2015**, *87*, 1051−1069.
(39) Bonilla, A.; Baudouin, D.; Pérez-Ramírez, J. Desilication of ferrierite zeolite for porosity generation and improved effectiveness in polyethylene pyrolysis. *J. Catal.* **2009**, *265*, 170−180.
(40) Verboekend, D.; Groen, J. C.; Pérez-Ramírez, J. Interplay of properties and functions upon introduction of mesoporosity in ITQ-4 Zeolite. *Adv. Funct. Mater.* **2010**, *20*, 1441−1450.
(41) Verboekend, D.; Caicedo-Realpe, R.; Bonilla, A.; Santiago, M.; Pérez-Ramírez, J. Properties and functions of hierarchical ferrierite zeolites obtained by sequential post-synthesis treatments. *Chem. Mater.* **2010**, *22*, 4679−4689.
(42) Niwa, M.; Katada, N. Measurements of acidic property of zeolites by temperature programmed desorption of ammonia. *Catal. Surv. Asia* **1997**, *1*, 215−226.
(43) Matias, P.; Couto, C. S.; Graca, I.; Lopes, J. M.; Carvalho, A. P.; Ribeiro, F. R.; Guisnet, M. Desilication of a TON zeolite with NaOH: Influence on porosity, acidity and catalytic properties. *Appl. Catal., A* **2011**, *399*, 100−109.
(44) del Campo, P.; Beato, P.; Rey, F.; Navarro, M. T.; Olsbye, U.; Lillerud, K. P.; Svelle, S. Influence of post-synthetic modifications on the composition, acidity and textural properties of ZSM-22 zeolite. *Catal. Today* **2018**, *299*, 120−134.
(45) Zhang, S.; Gong, Y.; Zhang, L.; Liu, Y.; Dou, T.; Xu, J.; Deng, F. Hydrothermal treatment on ZSM-5 extrudates catalyst for methanol to propylene reaction: Finely tuning the acidic property. *Fuel Process. Technol.* **2015**, *129*, 130−138.
(46) Tian, Y.; Zhang, B.; Liang, H.; Hou, X.; Wang, L.; Zhang, X.; Liu, G. Synthesis and performance of pillared HZSM-5 nanosheet zeolites for n-decane catalytic cracking to produce light olefins. *Appl. Catal., A* **2019**, *572*, 24−33.
(47) Borges, L. D.; Macedo, J. L. D. Solid-state dealumination of zeolite Y: Structural characterization and acidity analysis by calorimetric measurements. *Microporous Mesoporous Mater.* **2016**, *236*, 85−93.
(48) Wei, F.-F.; Cui, Z.-M.; Meng, X.-J.; Cao, C.-Y.; Xiao, F.-S.; Song, W.-G. Origin of the low olefin production over HZSM-22 and HZSM-23 Zeolites: External acid sites and pore mouth catalysis. *ACS Catal.* **2014**, *4*, 529−534.
(49) Bao, S.; Guo, M.; Liu, B.; Feng, B.; Yin, D.; Jiang, B.; Zhao, H. Effect of P sources on the phosphorus modified MCM-22 for n-hexane catalytic cracking. *React. Kinet., Mech. Catal.* **2021**, *132*, 431−447.
(50) Zhang, H.; Li, P.; Cui, W.; Liu, C.; Wang, S.; Zheng, S.; Zhang, Y. Synthesis of nanostructured γ-AlOOH and its accelerating behavior

https://doi.org/10.1021/acsomega.2c05478
ACS Omega 2023, 8, 14349−14364

on the thermal decomposition of AP. *RSC Adv.* **2016**, *6*, 27235−27241.
(51) Seo, Y. I.; Lee, Y. J.; Kim, D.-G.; Lee, K. H.; Kim, Y. D. Mechanism of aluminum hydroxide layer formation by surface modification of aluminum. *Appl. Surf. Sci.* **2010**, *256*, 4434−4437.
(52) Pérez-Ramírez, J.; Christensen, C. H.; Egeblad, K.; Christensen, C. H.; Groen, J. C. Hierarchical zeolites: enhanced utilisation of microporous crystals in catalysis by advances in materials design. *Chem. Soc. Rev.* **2008**, *37*, 2530−2542.
(53) Verboekend, D.; Pérez-Ramírez, J. Design of hierarchical zeolite catalysts by desilication. *Catal. Sci. Technol.* **2011**, *1*, 879−890.
(54) Serrano, D. P.; Escola, J. M.; Pizarro, P. Synthesis strategies in the search for hierarchical zeolites. *Chem. Soc. Rev.* **2013**, *42*, 4004−4035.
(55) Groen, J. C.; Jansen, J. C.; Moulijn, J. A.; Pérez-Ramírez, J. Optimal aluminum-assisted mesoporosity development in MFI zeolites by desilication. *J. Phys. Chem. B* **2004**, *108*, 13062−13065.
(56) Groen, J. C.; Moulijn, J. A.; Perez-Ramirez, J. Desilication: on the controlled generation of mesoporosity in MFI zeolites. *J. Mater. Chem.* **2006**, *16*, 2121−2131.
(57) Groen, J. C.; Peffer, L. A. A.; Moulijn, J. A.; Perez-Ramirez, J. Mechanism of hierarchical porosity development in MFI zeolites by desilication: The role of aluminium as a pore-directing agent. *Chem. − Eur. J.* **2005**, *11*, 4983−4994.
(58) Liu, H.; Liu, S. L.; Xie, S. J.; Song, C.; Xin, W. J.; Xu, L. Y. Effect of desilication on the performance of hierarchical ZSM-11 catalysts for alkylation of benzene with dimethyl ether. *Catal. Lett.* **2015**, *145*, 1972−1983.
(59) Zhang, K.; Fernandez, S.; Kobaslija, S.; Pilyugina, T.; O'Brien, J.; Lawrence, J. A.; Ostraat, M. L. Optimization of hierarchical structures for Beta zeolites by post-synthetic base leaching. *Ind. Eng. Chem. Res.* **2016**, *55*, 8567−8575.
(60) Groen, J. C.; Bach, T.; Ziese, U.; Paulaime-van Donk, A. M.; de Jong, K. P.; Moulijn, J. A.; Pérez-Ramírez, J. Creation of hollow zeolite architectures by controlled desilication of Al-zoned ZSM-5 crystals. *J. Am. Chem. Soc.* **2005**, *127*, 10792−10793.
(61) Li, T.; Ma, Z.; Krumeich, F.; Knorpp, A. J.; Pinar, A. B.; van Bokhoven, J. A. Properties modification of nanosized hollow zeolite crystals by desilication. *ChemNanoMat* **2018**, *4*, 992−999.
(62) Prates, A. R. M.; Chetot, T.; Burel, L.; Pagis, C.; Martinez-Franco, R.; Dodin, M.; Farrusseng, D.; Tuel, A. Hollow structures by controlled desilication of beta zeolite nanocrystals. *J. Solid State Chem.* **2020**, *281*, No. 121033.
(63) Verboekend, D.; Chabaneix, A. M.; Thomas, K.; Gilson, J.-P.; Pérez-Ramírez, J. Mesoporous ZSM-22 zeolite obtained by desilication: peculiarities associated with crystal morphology and aluminium distribution. *CrystEngComm* **2011**, *13*, 3408−3416.
(64) Verboekend, D.; Keller, T. C.; Milina, M.; Hauert, R.; Pérez-Ramírez, J. Hierarchy brings function: Mesoporous Clinoptilolite and L zeolite catalysts synthesized by tandem acid−base treatments. *Chem. Mater.* **2013**, *25*, 1947−1959.
(65) Wang, J.; Li, J.; Xu, S.; Zhi, Y.; Wei, Y.; He, Y.; Chen, J.; Zhang, M.; Wang, Q.; Zhang, W.; Wu, X.; Guo, X.; Liu, Z. Methanol to hydrocarbons reaction over HZSM-22 and SAPO-11: Effect of catalyst acid strength on reaction and deactivation mechanism. *Chin. J. Catal.* **2015**, *36*, 1392−1402.
(66) Bleken, F.; Bjørgen, M.; Palumbo, L.; Bordiga, S.; Svelle, S.; Lillerud, K.-P.; Olsbye, U. The effect of acid strength on the conversion of methanol to olefins over acidic microporous catalysts with the CHA topology. *Top. Catal.* **2009**, *52*, 218−228.
(67) Wang, Y.; Gao, Y.; Chu, W.; Zhao, D.; Chen, F.; Zhu, X.; Li, X.; Liu, S.; Xie, S.; Xu, L. Synthesis and catalytic application of FER zeolites with controllable size. *J. Mater. Chem. A* **2019**, *7*, 7573−7580.
(68) Pinar, A. B.; Márquez-Álvarez, C.; Grande-Casas, M.; Pérez-Pariente, J. Template-controlled acidity and catalytic activity of ferrierite crystals. *J. Catal.* **2009**, *263*, 258−265.
(69) Khitev, Y. P.; Ivanova, I. I.; Kolyagin, Y. G.; Ponomareva, O. A. Skeletal isomerization of 1-butene over micro/mesoporous materials based on FER zeolite. *Appl. Catal., A* **2012**, *441*−*442*, 124−135.
(70) Li, S.; Zheng, A.; Su, Y.; Zhang, H.; Chen, L.; Yang, J.; Ye, C.; Deng, F. Brønsted/Lewis acid synergy in dealuminated HY Zeolite: A combined solid-state NMR and theoretical calculation study. *J. Am. Chem. Soc.* **2007**, *129*, 11161−11171.
(71) Yu, Z.; Li, S.; Qiang, W.; Zheng, A.; Xu, J.; Lei, C.; Feng, D. Brønsted/Lewis acid synergy in H-ZSM-5 and H-MOR zeolites studied by ^{1}H and ^{27}Al DQ-MAS solid-state NMR spectroscopy. *J. Phys. Chem. C* **2011**, *115*, 22320−22327.
(72) Cañizares, P.; Carrero, A. Dealumination of ferrierite by ammonium hexafluorosilicate treatment: characterization and testing in the skeletal isomerization of n-butene. *Appl. Catal., A* **2003**, *248*, 227−237.
(73) Yu, Z.; Wang, Q.; Chen, L.; Deng, F. Brønsted/Lewis acid sites synergy in H-MCM-22 zeolite studied by ^{1}H and ^{27}Al DQ-MAS NMR spectroscopy. *Chin. J. Catal.* **2012**, *33*, 129−139.
(74) Kangas, M.; Kumar, N.; Harlin, E.; Salmi, T.; Murzin, D. Y. Skeletal isomerization of butene in fixed beds. 1. Experimental investigation and structure-performance effects. *Ind. Eng. Chem. Res.* **2008**, *47*, 5402−5412.
(75) Guisnet, M.; Andy, P.; Gnep, N. S.; Benazzi, E.; Travers, C. Skeletal isomerization of n-butenes. 1. Mechanism of n-butene transformation on a nondeactivated H-ferrierite catalyst. *J. Catal.* **1996**, *158*, 551−560.
(76) Guisnet, M. "Coke" molecules trapped in the micropores of zeolites as active species in hydrocarbon transformations. *J. Mol. Catal. A: Chem.* **2002**, *182*−*183*, 367−382.
(77) Guisnet, M.; Costa, L.; Ribeiro, F. R.; et al. Prevention of zeolite deactivation by coking. *J. Mol. Catal. A: Chem.* **2009**, *305*, 69−83.
(78) Lin, T. J.; Meng, X.; Shi, L. Ni-exchanged Y-zeolite: An efficient heterogeneous catalyst for acetylene hydrocarboxylation. *Appl. Catal., A* **2014**, *485*, 163−171.
(79) Zhang, X.; Wang, Y.; Xin, F. Coke deposition and characterization on titanium silicalite-1 catalyst in cyclohexanone ammoximation. *Appl. Catal., A* **2006**, *307*, 222−230.
(80) Xian, X.; Ran, C.; Nai, C.; Yang, P.; Zhao, S.; Dong, L. Characterization of the location of coke deposited on spent HZSM-5 zeolite by special temperature-programmed oxidation and isothermal oxidation methods. *Appl. Catal., A* **2017**, *547*, 37−51.
(81) Lin-Vien, D.; Colthup, N. B.; Fateley, W. G.; Grasselli, J. G. Alkanes. In *The Handbook of Infrared and Raman Characteristic Frequencies of Organic Molecules*, 1st ed.; Lin-Vien, D.; Colthup, N. B.; Fateley, W. G.; Grasselli, J. G., Eds.; Academic Press: New York, 1991; Chapter 2, pp 9−28.
(82) Aguayo, A. s. T.; Castaño, P.; Mier, D.; Gayubo, A. G.; Olazar, M.; Bilbao, J. Effect of cofeeding butane with methanol on the deactivation by coke of a HZSM-5 zeolite catalyst. *Ind. Eng. Chem. Res.* **2011**, *50*, 9980−9988.
(83) Li, J.; Xiong, G.; Feng, Z.; Liu, Z.; Xin, Q.; Li, C. Coke formation during the methanol conversion to olefins in zeolites studied by UV Raman spectroscopy. *Microporous Mesoporous Mater.* **2000**, *39*, 275−280.
(84) Campbell, S. M.; Bibby, D. M.; Coddington, J. M.; Howe, R. F.; Meinhold, R. H. Dealumination of HZSM-5 zeolites: I. Calcination and hydrothermal treatment. *J. Catal.* **1996**, *161*, 338−349.
(85) Fan, M.; Si, T.; Zhang, P. Effect of surface modification of H^{+}-Mordenite on the isomerization of oleic acid into branched-chain isomers. *J. Am. Oil Chem. Soc.* **2018**, *95*, 1357−1365.
(86) Li, X.; Tsai, S.-T.; Wu, K. C. W.; Curnow, O. J.; Choi, J.; Yip, A. C. K. Morphology control of ionic-liquid-templated ZSM-22 and ZSM-5 zeolites using a two-step process and its effect on toluene methylation. *Microporous Mesoporous Mater.* **2021**, *328*, No. 111475.
(87) Ayari, F.; Mannei, E.; Asedegbega-Nieto, E.; Mhamdi, M.; Guerrero-Ruiz, A. R.; Delahay, G.; Ghorbel, A. More insight on the isothermal spreading of solid MoO_3 into ZSM-5 zeolite. *React. Kinet., Mech. Catal.* **2018**, *124*, 419−436.
(88) Choudhary, V. R.; Pataskar, S. G. Stepwise thermal deammoniation of NH_4-Y and NH_4-ZSM-5 zeolites. *Mater. Chem. Phys.* **1985**, *13*, 587−592.

https://doi.org/10.1021/acsomega.2c05478
ACS Omega 2023, 8, 14349−14364

(89) Udovic, T. J.; Cavanagh, R. R.; Rush, J. J.; Wax, M. J.; Stucky, G. D.; Jones, G. A.; Corbin, D. R. Neutron scattering study of ammonium dynamics during the deammoniation of NH_4-rho zeolite. *J. Phys. Chem. A* **1987**, *91*, 5968−5973.
(90) Bernauer, M.; Tabor, E.; Pashkova, V.; Kaucky, D.; Sobalik, Z.; Wichterlova, B.; Dedecek, J. Proton proximity-New key parameter controlling adsorption, desorption and activity in propene oligomerization over H-ZSM-5 zeolites. *J. Catal.* **2016**, *344*, 157−172.
(91) Mlinar, A. N.; Zimmerman, P. M.; Celik, F. E.; Head-Gordon, M.; Bell, A. T. Effects of Brønsted-acid site proximity on the oligomerization of propene in H-MFI. *J. Catal.* **2012**, *288*, 65−73.

https://doi.org/10.1021/acsomega.2c05478
ACS Omega 2023, 8, 14349−14364